NAVAL POSTGRADUATE SCHOOL

MONTEREY, CALIFORNIA

THESIS

DESIGN AND ANALYSIS OF A SOLAR-POWERED COMPRESSED AIR ENERGY STORAGE SYSTEM

by

Thomas H. Prinsen

December 2016

Thesis Advisor: Anthony Gannon
Co-Advisor: Andrea Holmes

THIS PAGE INTENTIONALLY LEFT BLANK

REPORT DOCUMENTATION PAGE			*Form Approved OMB No. 0704–0188*

1. AGENCY USE ONLY *(Leave blank)*	**2. REPORT DATE** December 2016	**3. REPORT TYPE AND DATES COVERED** Master's thesis

4. TITLE AND SUBTITLE
DESIGN AND ANALYSIS OF A SOLAR-POWERED COMPRESSED AIR ENERGY STORAGE SYSTEM

5. FUNDING NUMBERS

6. AUTHOR(S) Thomas H. Prinsen,

7. PERFORMING ORGANIZATION NAME(S) AND ADDRESS(ES)
Naval Postgraduate School
Monterey, CA 93943-5000

8. PERFORMING ORGANIZATION REPORT NUMBER

9. SPONSORING /MONITORING AGENCY NAME(S) AND ADDRESS(ES)
Project supported by the Office of Naval Research's (ONR) Energy Systems Technology Evaluation Program (ESTEP), supported by Dr. Richard Carlin and under the technical monitoring of Stacey Curtis.

10. SPONSORING / MONITORING AGENCY REPORT NUMBER

11. SUPPLEMENTARY NOTES The views expressed in this thesis are those of the author and do not reflect the official policy or position of the Department of Defense or the U.S. Government. IRB number ____N/A____.

12a. DISTRIBUTION / AVAILABILITY STATEMENT
Approved for public release. Distribution is unlimited.

12b. DISTRIBUTION CODE

13. ABSTRACT (maximum 200 words)

This thesis is a two-party study that analyzed a compressed air storage system using fundamental thermodynamic principles and designed the compression phase using commercial-off-the-shelf components. The analysis for this system used a novel control-mass methodology that allowed both isentropic and isothermal work and heat transfer processes to be calculated using end states. The resulting formulas provide a rigorously derived yet straightforward benchmark for the upper limits of efficiency in such systems.

The design portion of this study lays the groundwork for building the compression phase of a solar-powered compressed air energy storage system that will integrate a rotary compressor, ultracapacitors, and a turbocharger to serve as proof-of-concept for an environmentally friendly energy storage system that can effectively utilize energy provided by solar radiation. Once implemented, this system's practicality has the potential to spur the use of solar panels on Department of Defense shore installations without the side effect of relying on rare-earth materials for energy storage.

14. SUBJECT TERMS compressed air, benchmark, efficiency, solar, energy storage	**15. NUMBER OF PAGES** 89
	16. PRICE CODE

17. SECURITY CLASSIFICATION OF REPORT	**18. SECURITY CLASSIFICATION OF THIS PAGE**	**19. SECURITY CLASSIFICATION OF ABSTRACT**	**20. LIMITATION OF ABSTRACT**
Unclassified	Unclassified	Unclassified	UU

NSN 7540–01-280-5500 Standard Form 298 (Rev. 2–89)
Prescribed by ANSI Std. 239–18

THIS PAGE INTENTIONALLY LEFT BLANK

Approved for public release. Distribution is unlimited.

DESIGN AND ANALYSIS OF A SOLAR-POWERED COMPRESSED AIR ENERGY STORAGE SYSTEM

Thomas H. Prinsen
Lieutenant, United States Navy
B.S., University of Kansas, 2010

Submitted in partial fulfillment of the
requirements for the degree of

MASTER OF SCIENCE IN MECHANICAL ENGINEERING

from the

NAVAL POSTGRADUATE SCHOOL
December 2016

Approved by: Anthony Gannon
Thesis Advisor

Andrea Holmes
Co-Advisor

Garth Hobson
Chair, Department of Mechanical and Aerospace Engineering

THIS PAGE INTENTIONALLY LEFT BLANK

ABSTRACT

This thesis is a two-part study that analyzed a compressed air storage system using fundamental thermodynamic principles and designed the compression phase using commercial-off-the-shelf components. The analysis for this system used a novel control-mass methodology that allowed both isentropic and isothermal work and heat transfer processes to be calculated using end states. The resulting formulas provide a rigorously derived yet straightforward benchmark for the upper limits of efficiency in such systems.

The design portion of this study lays the groundwork for building the compression phase of a solar-powered compressed air energy storage system that will integrate a rotary compressor, ultracapacitors, and a turbocharger to serve as proof-of-concept for an environmentally friendly energy storage system that can effectively utilize energy provided by solar radiation. Once implemented, this system's practicality has the potential to spur the use of solar panels on Department of Defense shore installations without the side effect of relying on rare-earth materials for energy storage.

THIS PAGE INTENTIONALLY LEFT BLANK

TABLE OF CONTENTS

THIS PAGE INTENTIONALLY LEFT BLANK

LIST OF FIGURES

THIS PAGE INTENTIONALLY LEFT BLANK

LIST OF TABLES

THIS PAGE INTENTIONALLY LEFT BLANK

LIST OF ACRONYMS AND ABBREVIATIONS

AA-CAES	advanced adiabatic compressed air energy storage
CAES	compressed air energy storage
COTS	commercial-off-the-shelf
DON	Department of the Navy
IMPREL	Integrated Multi-Physics Renewable Energy Lab
MPPT	maximum power point tracking
NPS	Naval Postgraduate School
PV	Photovoltaic
SECNAV	Secretary of the Navy
SS-CAES	small scale compressed air energy storage
TES	thermal energy storage

THIS PAGE INTENTIONALLY LEFT BLANK

NOMENCLATURE

Symbol	Description	Units
c_p	constant-pressure specific heat capacity	[J/kg*k]
c_v	constant-volume specific heat capacity	[J/kg*K]
p	pressure	[Pa]
q	specific heat flow	[kJ/kg]
Q	volumetric flow rate	[m^3/s]
R_{air}	gas constant for air	[J/kg*K]
t	time	[s]
T	temperature	[K]
v	specific volume	[m^3/kg]
V	volume	[m^3]
w	specific work	[kJ/kg]
W	work	[kJ]
$\dot{w}$	specific power	[kW/kg/s]
$\dot{W}$	power	[kW]
γ	ratio of specific heat capacities	[dimensionless]
η	thermal efficiency	[dimensionless]

THIS PAGE INTENTIONALLY LEFT BLANK

LIST OF SUBSCRIPTS

1	state 1
2	state 2
3	state 3
4	state 4
air	air
atm	atmosphere
hp	high pressure
s	isentropic
tank	tank
th	isothermal

THIS PAGE INTENTIONALLY LEFT BLANK

ACKNOWLEDGMENTS

To my advisor, Dr. Gannon, I offer my sincere gratitude for the starting vision for this research, as well as the many helpful suggestions along the way. I also thank my mother and my late father for instilling in me a strong work ethic that has allowed me to get this far in the Navy.

A huge thank you to my wife, Krystal, who has endured many late nights and continues to keep our family growing strong. Your love and support have also allowed me to prosper throughout my naval career. You mean the world to me.

Finally, I must acknowledge the assistance I receive every day from my Lord and Savior, Jesus Christ.

Many are the plans in the mind of a man,
but it is the purpose of the LORD that will stand.

—Proverbs 19:21 (ESV)

THIS PAGE INTENTIONALLY LEFT BLANK

I. INTRODUCTION

This project is sponsored by the Office of Naval Research (ONR) as part of its Energy Systems Technology Evaluation Program (ESTEP). Through ESTEP, ONR partners with education and research facilities to "conduct real-world advanced technology demonstrations to evaluate emerging [clean] energy technologies using Navy and Marine Corps facilities as test beds" [1]. The system—a solar-powered small-scale compressed air energy storage (SS-CAES) system—is being designed using the multi-physics approach to energy storage, a "methodology that suggests design alternatives based on first principles and consideration of what the end-use of the energy storage will be," [2] and will be implemented at the Integrated Multi-Physics Renewable Energy Lab (IMPREL).

A. MOTIVATION

Renewable energy resources have been in use commercially for hundreds of years, but the focus on and demand for these resources have grown substantially since the turn of the century [3]. As Figure 1 indicates, the use of renewable and alternative energy sources is expected to nearly double in the next 20 years [4]. This growth is due in large part to the detrimental environmental side effects of current energy production methods, such as the rise in global average surface temperature [5]. These side effects have already driven much of the world's industrialized nations to implement legislative measures to curb the production of CO_2 and other greenhouse gases [6]. Although energy companies bear the majority of these regulations, the increased attention by the general public towards "going green" compels many other companies and organizations nationwide to alter their business practices as well [7].

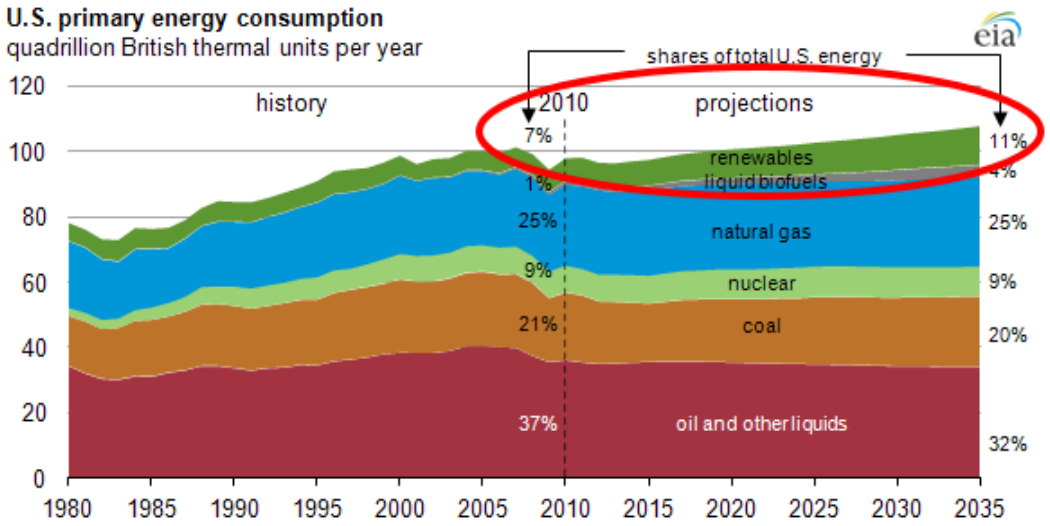

Figure 1. Projection of U.S. Energy Consumption by Energy Source. Adapted from [4].

The military is also interested in efficient use of renewable resources, largely because of diminishing supply and rising costs of fossil fuels. As Figure 2 shows, the U.S. Department of Defense (DOD) energy usage dwarfs that of any other organization in the world, and it is therefore very susceptible to increased fuel costs. Fuel cost volatility and its impact on the uncertainty in energy security has cast such a large shadow over mission readiness that the military has already taken steps to switch its own energy usage over to renewable resources. For the Navy, specifically, one of the five "Secretary of the Navy Energy Goals" is that, "by 2020, [the Department of the Navy (DON)] will produce 50 percent of shore-based energy requirements from alternative sources [8]. To promote fulfillment, SECNAV charged each region and installation with developing an energy plan [9]. In accordance with this strategy, COMNAVREGSWINST 4101.lA, the energy management plan for Naval Postgraduate School's (NPS) host region Navy Region Southwest, states that "installations shall develop on base micro-grids of renewable power" to replace the existing grid [10].

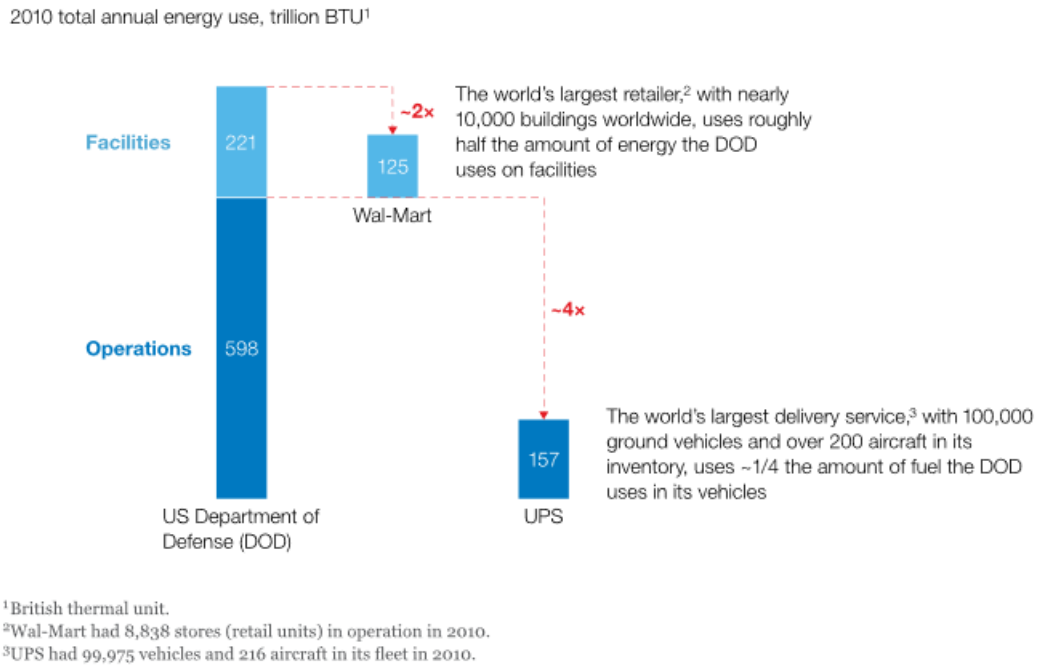

Figure 2. FY2010 U.S. DOD Energy Usage Compared against World's Largest Retailer and World's Largest Delivery Service. Source: [11].

B. LITERATURE REVIEW

Numerous studies have concluded that the growth in the use of renewable energy sources brings with it a need for energy storage technologies to smooth out the fluctuations in power generation caused by environmental variability [12-14]. In the case of solar panels, power production occurs during daylight hours, which typically occurs when residents are not drawing a big electrical load because much of the household is not at home. Conversely, during nighttime hours, when lights are on and residents are in general using more electricity, the solar panels are sitting idle. Thus, without appropriate energy storage methods, excess power generation cannot be saved for later use. Compressed air energy storage (CAES) plants offer one solution to this obstacle with the ability to convert off-peak reduced-cost grid electricity (or any form of renewable energy with an inherently variable output) to stored energy in the form of high-pressure air. When electricity demand signal grows, this compressed air can be converted back to electricity by an expansion device. More broadly, compressed air itself "is used in thousands of applications and is vital to the productivity of industries around the globe" [15].

Figure 3 shows that—apart from pumped hydroelectric storage (PHS)—large-scale CAES offers the best energy storage method for energy management, defined as "the ability to shift bulk energy over periods of several hours or more" [13]. The main advantage CAES has over PHS is that it is not as severely constrained by geographic requirements. Another advantage for CAES was proposed by a recent study by Barnhart and Benson [16], which concluded that CAES actually surpasses PHS and is also vastly superior to electrochemical batteries as measured by energy stored on invested (ESOI), which is "the ratio of electrical energy stored over the lifetime of a storage device to the amount of primary embodied energy required to build the device." This conclusion, illustrated in Figure 4, means electrochemical battery cycle life must improve considerably before utilities will consider implementing them as a "load-balancing solution at global scale" [16]. Table 1 shows the immense size, weight, and cost of today's most advanced batteries when built to store 24 hours of electricity generation in the United States (based on data from [17]) [18].

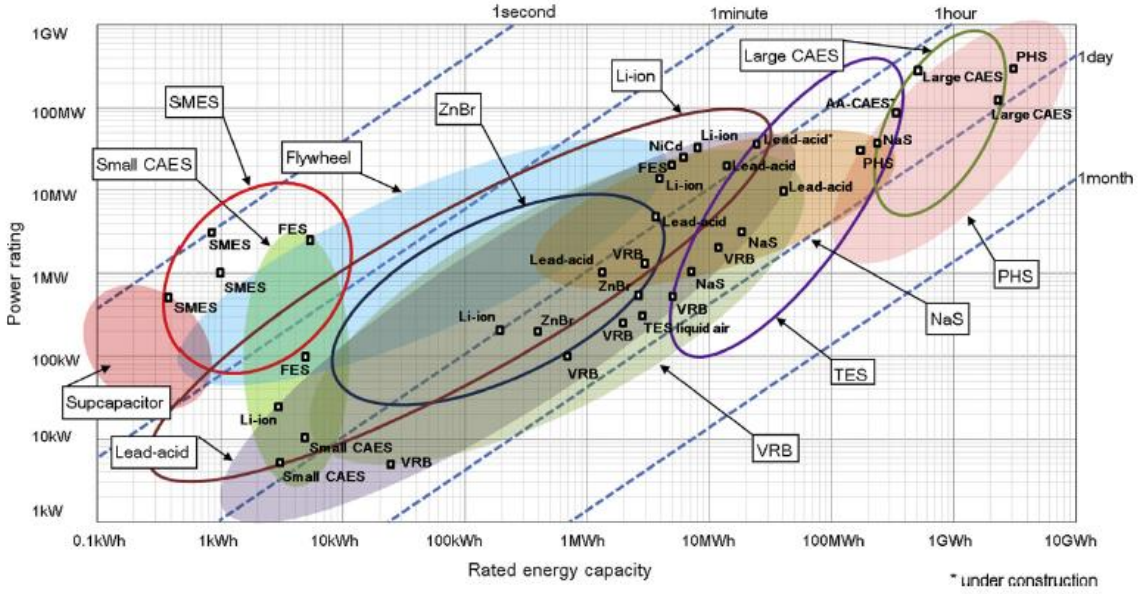

Figure 3. Comparison of Power Rating and Rated Energy Capacity with Discharge Time Duration at Rated Power. Source: [14].

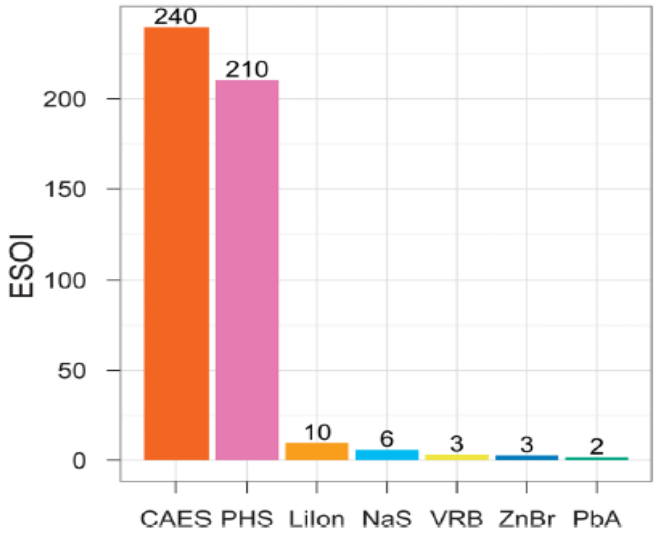

Figure 4. Bar Plot Showing ESOI for Load-Balancing Storage Technologies. Source: [16].

Table 1. Characteristics for Top Three Electrochemical Battery Technologies. Adapted from [18].

Battery	Size (square miles)	Weight (millions of tons)	Cost
Sodium Sulfur (NaS)	923	450	$40.77 trillion
Lithium-ion	345	74	$_11.9 trillion
Lead acid (advanced)	217.5	15.8	$8.3 trillion

These characteristics apply when building each battery to store 24 hours of U.S. energy production.

As Figure 5 shows, CAES cycle efficiency is not as high as that of PHS, but, as previously mentioned, geographic constraints have stalled PHS plant construction. Furthermore, the data in Figure 6 show that current power plants only operate at 33% efficiency, which means that CAES plants are actually more efficient than their fossil-fuel or nuclear counterparts. However, even though PV costs have dropped significantly in recent years, cycle efficiency continues to be the focus of many research papers. Grazzini and Milazzo [19, 20] performed a thermodynamic and exergy analysis of a theoretical CAES plant which uses thermal energy storage (TES) to lower compressor exit temperature (also known as advanced adiabatic CAES, or AA-CAES) and proposed

that cycle efficiency could be improved enough to make CAES competitive with other energy storage systems. Studies performed by the Arizona Research Institute for Solar Energy (AzRISE) [21] and Mason et al. [22] also found that TES would be needed to make solar-powered CAES cost effective against natural gas plants in regards to shaving peak costs during electric grid operations. However, these same studies stated that the timeline to utility scale implementation would be significantly affected by the dichotomy between natural gas prices and climate change concerns [21, 22]. In an effort to standardize research methods for future AA-CAES projects, various thermodynamic models of both large and small scale AA-CAES systems have been developed [23-25].

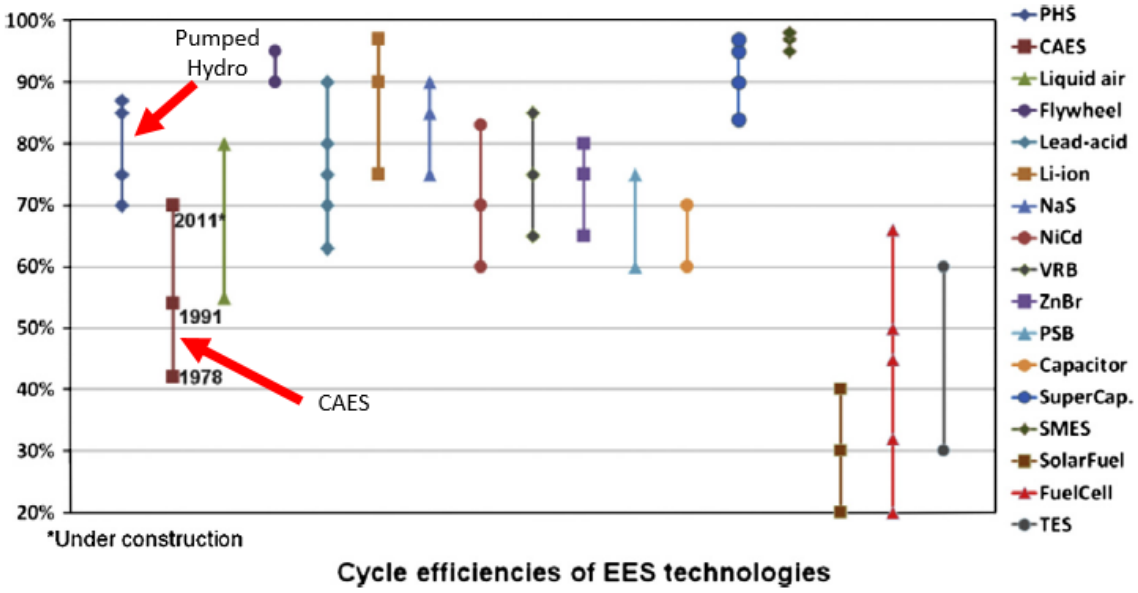

Figure 5. Comparison of Cycle Efficiencies for Various Energy Storage Systems. Adapted from [14].

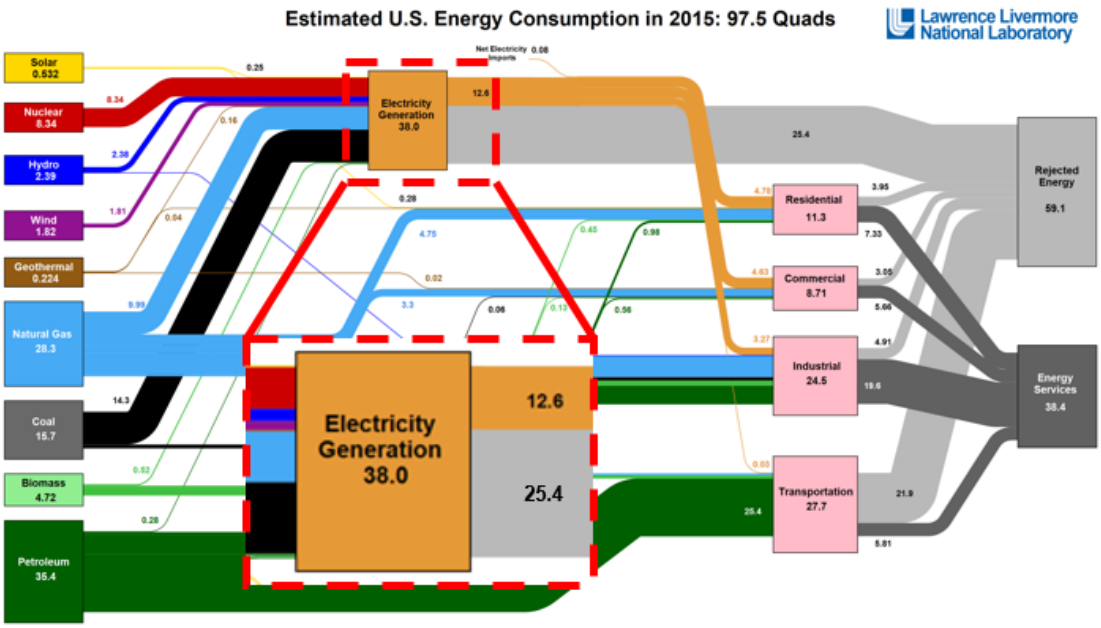

Figure 6. U.S. Energy Sources and Consumption Sectors in 2015. Adapted from [26].

1. Utility Scale Plants

Interest in CAES systems began in the late 1940s [27], but did not grow substantially until the 1970s as the cost of oil and gas increased significantly [28]. The first utility scale CAES system, a 290 MW plant near Huntorf, Germany, has been operating since 1978 and is currently being utilized to level the variable electricity generation of multiple wind turbines across Germany [29]. Following that, a 110 MW plant near McIntosh, Alabama, was started up in 1991 and is used primarily for load management and peak power generation [29]. Both plants use large underground caverns to store the compressed air and heat the compressed air with natural gas just prior to the power-producing expansion phase. Of note, these two plants come in second only to PHS in terms of providing worldwide grid-scale energy storage [30].

Up until just a few years ago, the growth in research and development for the CAES concept has been held stagnant by geographic constraints as well as economical oil and natural gas prices. A handful of startup companies have begun making CAES plants fossil-fuel free by using renewable energy to compress the air and have been

testing designs that would make the compression and storage phases more efficient. In 2013, Apex Compressed Air Energy Storage announced plans to collaborate with Dresser-Rand to build a 317-MW plant in salt caverns near Dallas, Texas. Dresser-Rand, the same company who had built equipment for the Alabama CAES plant, was planning to use its newly developed "integrated energy storage technology, called SMART*CAES*" in the Texas plant [31]. However, as of late 2014, these plans had been placed on hold indefinitely [32].

Also in 2013, SustainX built a 1.5-MW demonstration plant that attempted to both improve thermal efficiency by spraying water into the air to achieve near-isothermal compression and remove the geographic constraint by storing the air-water mix in above-ground pipes, similar to those used by the natural gas industry [33]. This above-ground approach failed to meet expectations, and in 2015, SustainX merged with General Compression, a company with a 2-MW plant in Texas that uses salt caverns to store air compressed by a wind turbine [34].

LightSail Energy (LSE) is also attempting to revolutionize the above-ground approach to CAES. As with SustainX's original approach, LSE is injecting a water mist into the compression chamber to improve thermal efficiency, as shown in Figure 7 [35]. To lower the costs of the storage system, it is developing carbon-fiber tanks [36]. As of 2015, LSE is working on two field projects: one in Canada will store energy produced from a wind turbine, and the other at Naval Base Ventura County in California will store energy produced from photovoltaic (PV) panels [36, 37].

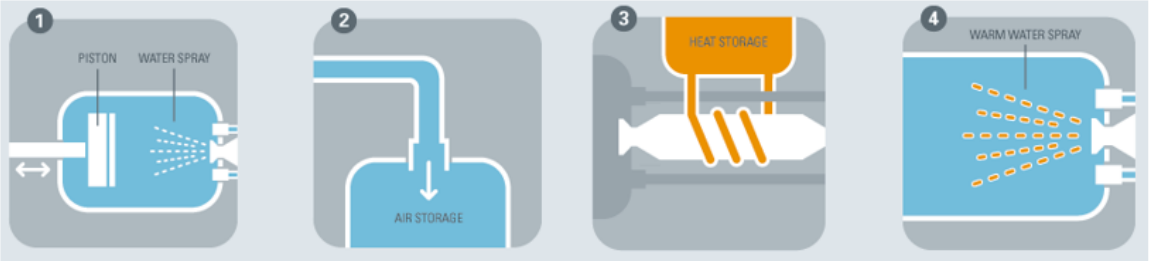

Figure 7. Overview of LightSail Energy's Compressed Air Energy Storage System. Adapted from [35].

In a slightly different approach, a company based in England called Isentropic stores the heat generated from compression of air in a layered bed of crushed gravel [38]. This new thermal storage concept and the reciprocating heat pumps that were built for this energy storage system are collectively termed Pumped Heat Energy Storage (PHES) [38]. A screenshot of a video showing the compression phase of this storage system is shown in Figure 8. By using highly efficient heat pumps and a set of control valves to ensure only a relatively small volume of crushed gravel is being actively cooled/heated, the company claims PHES will reach an efficiency on par with pumped hydro-electric energy storage [38].

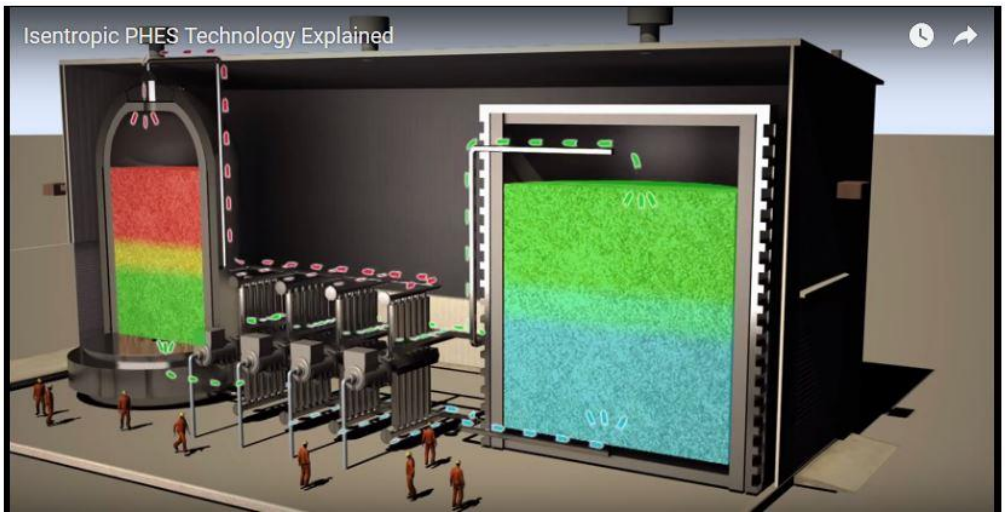

Figure 8. Screenshot of Isentropic Company Video Showing Compression Phase of PHES System. Source: [39].

2. Medium- and Small-Scale Research

The geographic constraints imposed on the underground approach to large scale CAES has caused engineers and economists to also analyze various forms of medium- and small-scale CAES systems. Petrov et al. [40] proposed a distributed network of CAES systems that would be more environmentally friendly than current battery technology and, under the appropriate control strategy, could either work with the grid or be isolated to individual residences. Kim et al. [41, 42] developed a patent for a system that combines CAES with PHS by utilizing two tanks. As shown in Figure 9, one tank is

for air storage and the other is for hydraulic energy storage to maintain the compressed air at constant pressure to avoid the efficiency losses inherent in pressure regulation.

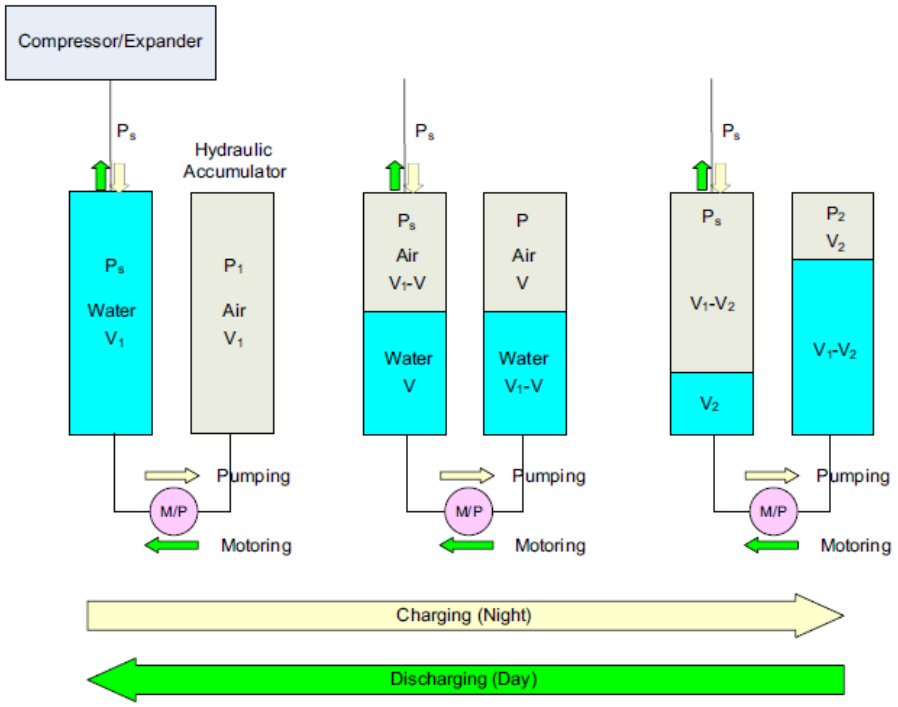

Figure 9. Operation of Constant-Pressure CAES System Combined with Hydraulic Energy Storage. Source: [41].

In terms of backup power, CAES can be combined with other energy storage technologies such as flywheels or supercapacitors to produce an Uninterruptible Power Supply system that offers both an excellent response time and extended runtime [43, 44]. For remote areas, Ibrahim et al. [45] have proposed a hybrid system that supplements power supplied by a diesel generator with air compressed by a wind turbine powered compressor.

Regarding stand-alone CAES systems, a team from the University of Kansas developed a CAES system prototype powered by a shrouded wind turbine to demonstrate the concept that these systems could be scaled down to help power individual residences [46]. Paloheimo and Omidiora [47] analyzed the feasibility of using CAES and micro turbines to power personal electronic devices in third world countries. Villela et al. [48]

focused their research on the compression stage and developed a "low-power high efficiency" compressor prototype that was specifically designed to work with residential-sized PV panel arrays. Kim et al. [49] and Manfrida et al. [50] proposed that a SS-AA-CAES system using COTS parts could be made more economical by using the heat generated from the compression stage and the cooling that takes place during the expansion stage for residential heating and cooling. Keeney [51] scrutinized efficiency claims by various industrial companies and collected rudimentary experimental data by testing a SS-CAES system using commercial-off-the-shelf (COTS) parts.

C. PROJECT OBJECTIVES

This thesis is a two-part study that details the design and analysis of a solar-powered SS-CAES. The primary objective for implementing a solar-powered compression system is to replace an aging compression system used solely to charge a supersonic wind tunnel. A secondary objective is to integrate this compression system into a bigger study that aims to develop a proof-of-concept SS-CAES system that utilizes a small-scale generator for the expansion phase (developed by Mclaughlin [52]). Despite the many research papers that discuss CAES system capability and practicality, the literature review has shown that building a solar-powered SS-CAES system with COTS parts would take the CAES research field a significant step forward. The objective for the design portion of this study is to find COTS parts for a compression system that operates within the parameters allowed by a micro grid that is presently installed at the IMPREL.

The analysis for this system uses a novel control-mass methodology that allows both isentropic and isothermal work and heat transfer processes to be calculated using end states. The objective for this analysis is to provide a rigorously-derived yet straightforward benchmark for the upper limits of efficiency in CAES systems.

THIS PAGE INTENTIONALLY LEFT BLANK

II. THERMODYNAMICS OF CAES MODEL

Current thermodynamic models for compressed air energy storage systems employ the steady-flow-open-system approach, which relies on describing how gas properties incrementally change as air pressure builds up in the storage vessel [23, 24, 53]. This approach, while technically correct, tends to be tedious and time-consuming and does not lead to insight into the system operation.

To describe this energy storage system using the fundamental concepts of the First Law of Thermodynamics, a control mass, state-based approach was developed in which the compression and expansion processes were both modelled as utilizing a long piston-cylinder arrangement such that the mass of air needed to achieve the desired system pressure was contained within the initial volume of the storage tank and attached cylinder. This approach is conceptually illustrated in Figure 10.

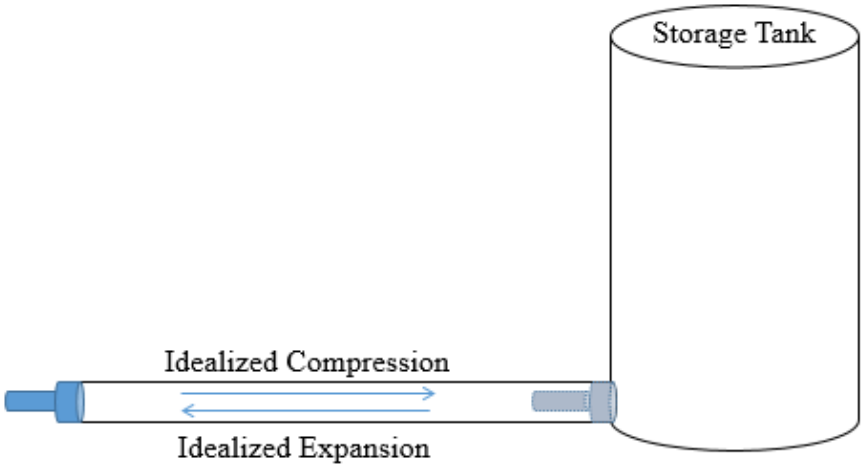

This diagram is not to scale.

Figure 10. System Diagram for Control Mass CAES System Approach.

To preserve the fundamental nature of this system's analysis, the following assumptions were applied:

- The working fluid, air, behaves as an ideal gas.

- Pressure loss in pipe flows and kinetic and potential energy effects of the gas flow are negligible.
- The compression phase begins with, and the expansion phase ends at, atmospheric conditions.

These assumptions allow use of the Ideal Gas Law, simplify use of the First Law of Thermodynamics, and allow for a cycle analysis. The system was first analyzed using isentropic work processes; an isothermal cycle was then analyzed to form a reference.

A. ISENTROPIC CYCLE ANALYSIS

To compute the energy added to and subsequently extracted from the system on a per mass basis by the compression and expansion phases using the state-based approach for an isentropic cycle, the work and heat transfer processes were separated and analyzed independently. Figure 11 shows that this separation produces processes that are analogous to the Atkinson air standard cycle. Figure 12 and 13 illustrate the processes and the four distinct states:

- State 1 (dotted-line control mass of Figure 12 and compound-dashed-line control mass of Figure 13) describes the air at atmospheric pressure and temperature, p_{atm} and T_{atm}, respectively, within an initial volume, V_1 (both before isentropic compression and after constant-pressure atmospheric heat absorption).
- State 2 (dashed-line control mass of Figure 12) describes the air at the pressure, p_2, and temperature, T_2, that would be reached after it has been isentropically compressed from State 1 to the volume of the storage tank, V_{tank}, assuming the tank and cylinder had perfect thermal insulation.
- State 3 (dashed-line control mass of Figures 12 and 13) describes the air at the desired high pressure, p_{hp}, after it has undergone constant-volume atmospheric heat loss to T_{atm}.
- State 4 (dotted-line control mass of Figure 13) describes the air at the volume, V_4, and temperature, T_4, that would be reached after it has been isentropically expanded from p_{hp} down to p_{atm}, assuming the tank and cylinder had perfect thermal insulation.

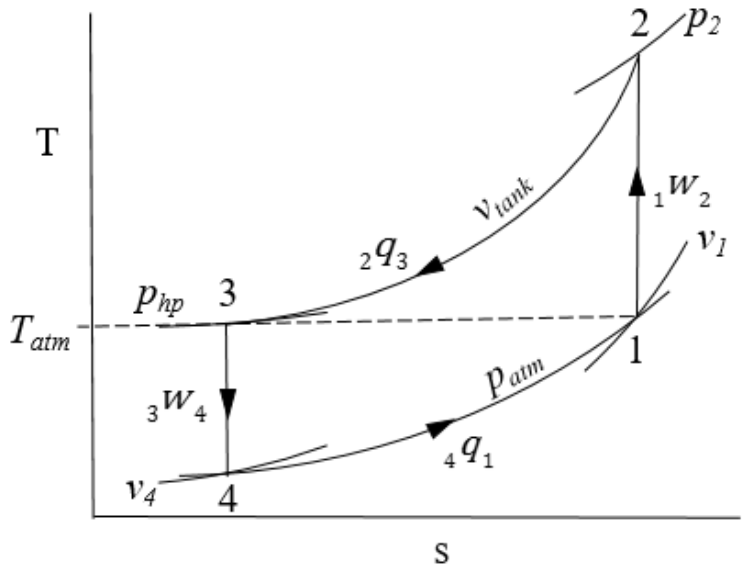

Figure 11. Temperature-Entropy Diagram for Isentropic CAES System Cycle.

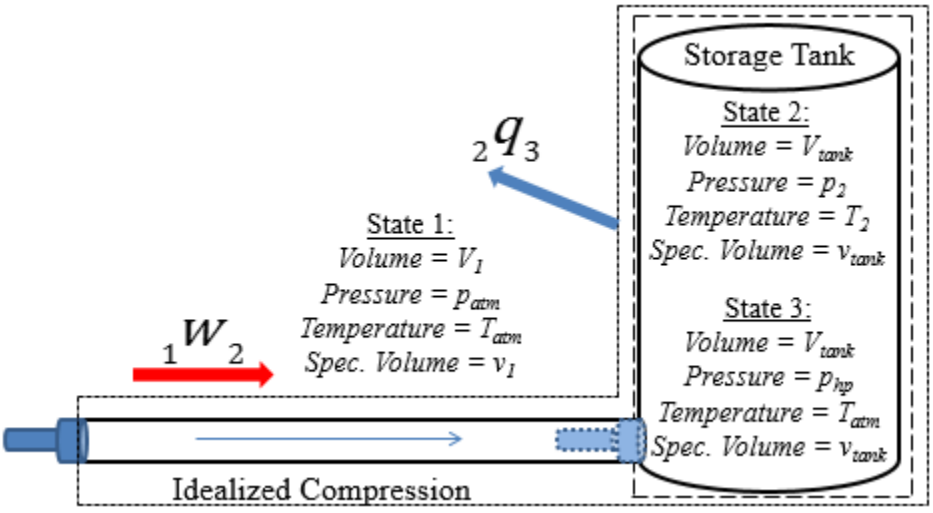

Figure 12. System Diagram Showing Processes and States for Isentropic Compression Phase.

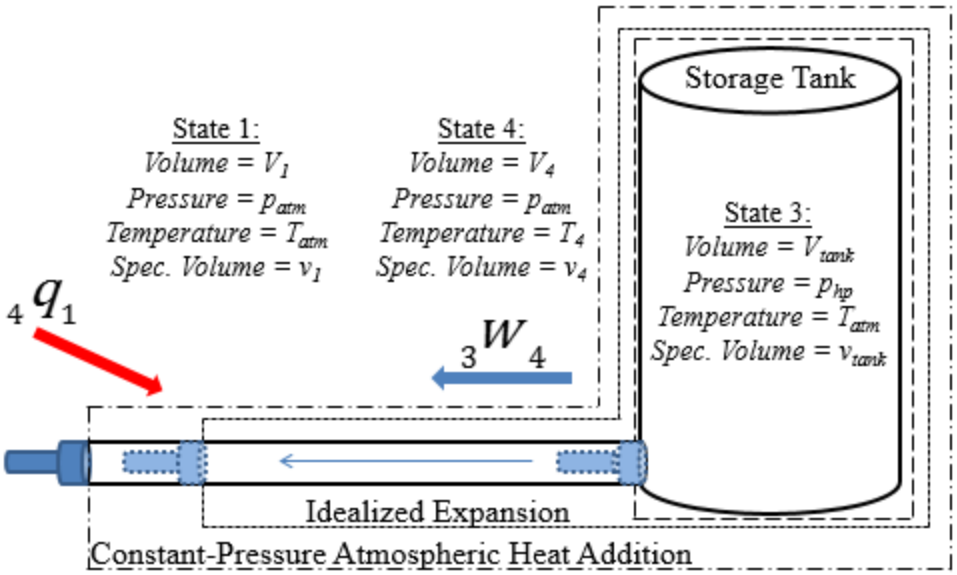

Figure 13. System Diagram Showing Processes and States for Isentropic Expansion Phase.

This system's thermal efficiency is defined as

$$\eta = \left| \frac{\text{Expansion Work Out}}{\text{Compression Work In}} \right| = \left| \frac{{}_3W_4}{{}_1W_2} \right| \tag{1}$$

As shown in Figure 11, ${}_1W_2$ is assumed to be an isentropic process. This allows the relationship between pressure and specific volume to be described as

$$p_1 v_1^{\gamma} = p_2 v_2^{\gamma} = constant \tag{2}$$

where γ is the ratio of specific heats. Equation (2) in turn allows ${}_1W_2$ to be calculated as

$${}_1W_2 = \int_1^2 p dv = \frac{1}{(1-\gamma)}\left(p_2 v_2 - p_1 v_1\right) \tag{3}$$

Figures 11 and 12 show that $p_1 = p_{atm}$ and $v_2 = v_{tank}$ for ${}_1W_2$. To determine v_1, the Ideal Gas Law was applied to state 1 as

$$v_1 = \frac{R_{air} T_{atm}}{p_{atm}} \tag{4}$$

To determine p_2, the Ideal Gas Law was first applied to state 3 as

$$T_3 = \frac{p_{hp} v_{tank}}{R_{air}} = T_{atm} \tag{5}$$

Substituting the right-hand side of Equation (5) into Equation (4) results in

$$v_1 = v_{tank} \frac{p_{hp}}{p_{atm}} \tag{6}$$

With v_1 known, Equation (2) is solved for p_2 as

$$p_2 = p_1 \left(\frac{v_1}{v_2} \right)^{\gamma} = p_{atm} \left(\frac{p_{hp}}{p_{atm}} \right)^{\gamma} \tag{7}$$

and thus ${}_1w_2$ becomes

$$\begin{aligned}
{}_1w_2 &= \frac{1}{(1-\gamma)} \left(p_{atm} \left(\frac{p_{hp}}{p_{atm}} \right)^{\gamma} v_{tank} - p_{atm} v_{tank} \frac{p_{hp}}{p_{atm}} \right) \\
&= \frac{1}{(1-\gamma)} \left(p_{atm} \left(\frac{p_{hp}}{p_{atm}} \right)^{\gamma} \frac{R_{air} T_{atm}}{p_{hp}} - R_{air} T_{atm} \right) \\
&= \frac{R_{air} T_{atm}}{p_{hp}} \frac{1}{(1-\gamma)} \left(p_{atm} \left(\frac{p_{hp}}{p_{atm}} \right)^{\gamma} - p_{hp} \right) \\
&= R_{air} T_{atm} \frac{1}{(1-\gamma)} \left(\left(\frac{p_{hp}}{p_{atm}} \right)^{\gamma-1} - 1 \right)
\end{aligned} \tag{8}$$

As with ${}_1w_2$, Figure 11 shows that ${}_3w_4$ is also an isentropic process, and is calculated as

$$ {}_3w_4 = \int_3^4 p dv = \frac{1}{(1-\gamma)}\left(p_4 v_4 - p_3 v_3\right) \tag{9} $$

where $p_3 = p_{hp}$ and $v = v_{tank}$. The pressure at state 4 (the end state of work due to expansion) is limited to p_{atm} since the atmosphere would push back on the piston if the system pressure dropped below p_{atm}. This limitation results in v_4 being less than v_1 and therefore must be determined using the isentropic pressure-volume relationship. Thus, v_4 is calculated as

$$ v_4 = \left(\frac{p_{hp}}{p_{atm}}\right)^{\frac{1}{\gamma}} v_{tank} \tag{10} $$

and ${}_3w_4$ becomes

$$ \begin{aligned} {}_3w_4 &= \frac{1}{(1-\gamma)}\left(p_{atm}\left(\frac{p_{hp}}{p_{atm}}\right)^{\frac{1}{\gamma}} v_{tank} - p_{hp} v_{tank}\right) \\ &= \frac{1}{(1-\gamma)}\left(p_{atm}\left(\frac{p_{hp}}{p_{atm}}\right)^{\frac{1}{\gamma}} \frac{R_{air} T_{atm}}{p_{hp}} - p_{hp}\frac{R_{air} T_{atm}}{p_{hp}}\right) \\ &= R_{air} T_{atm}\frac{1}{(1-\gamma)}\left(\left(\frac{p_{hp}}{p_{atm}}\right)^{\frac{1-\gamma}{\gamma}} - 1\right) \end{aligned} \tag{11} $$

Substituting the right-hand side of Equations (8) and (11) into Equation (1) results in a cycle thermal efficiency of

$$\eta = \left| \frac{R_{air} T_{atm} \frac{1}{(1-\gamma)} \left(\left(\frac{p_{hp}}{p_{atm}} \right)^{\frac{1-\gamma}{\gamma}} - 1 \right)}{R_{air} T_{atm} \frac{1}{(1-\gamma)} \left(\left(\frac{p_{hp}}{p_{atm}} \right)^{\gamma-1} - 1 \right)} \right|$$

$$= \left| \frac{\left(\left(\frac{p_{hp}}{p_{atm}} \right)^{\frac{1-\gamma}{\gamma}} - 1 \right)}{\left(\left(\frac{p_{hp}}{p_{atm}} \right)^{\gamma-1} - 1 \right)} \right| \qquad (12)$$

Figure 14 illustrates the relationship between the magnitude of isentropic specific compression and expansion work. Figure 15 shows cycle efficiencies for a system pressure range of just above atmospheric pressure (where the thermodynamic constraint imposed on ${}_3w_4$ results in a significant loss of efficiency despite the relatively small amounts of work) to 13.78 bar (200 psia). For a desired system pressure of 10.34 bar (150 psia) (the operating pressure for the proposed system), the cycle efficiency is approximately 33%, meaning the system could recover 33% of the energy put into it when operating isentropically.

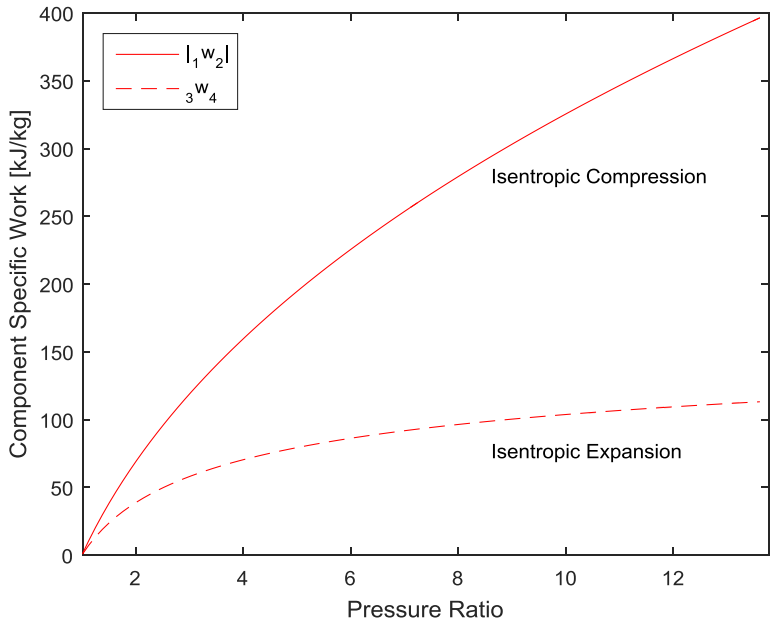

Figure 14. Component Isentropic Specific Work Based on System Pressure.

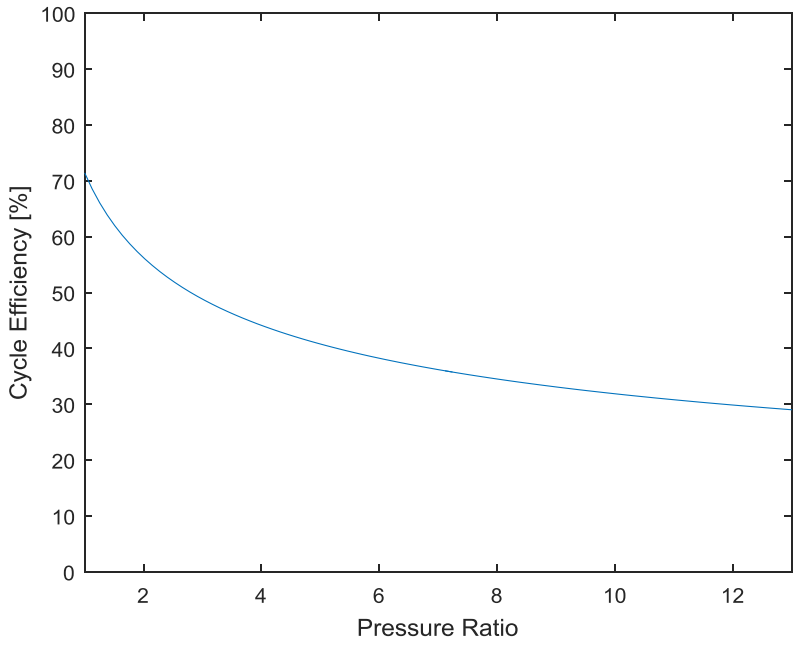

Figure 15. Cycle Thermal Efficiency Based on System Pressure.

Turning to analyze heat transfer, Figure 11 shows that the heat transfer for the compression phase is a constant-volume process that cools the air from the high temperature produced by the isentropic work process (state 2) down to T_{atm} (state 3). The specific heat transfer is thus calculated as

$$_2q_3 = c_v\left(T_3 - T_2\right) = c_v\left(T_{atm} - T_2\right) \tag{13}$$

T_2 can be written in terms of pressure by using the following isentropic pressure-temperature relationship, applied between states 1 and 2:

$$\frac{p_1}{p_2} = \left(\frac{T_1}{T_2}\right)^{\frac{\gamma}{\gamma-1}} \rightarrow \frac{p_{atm}}{p_2} = \left(\frac{T_{atm}}{T_2}\right)^{\frac{\gamma}{\gamma-1}} \tag{14}$$

Equation (14) can be rearranged to solve for T_2 as

$$T_2 = \left(\frac{p_2}{p_{atm}}\right)^{\frac{\gamma-1}{\gamma}} T_{atm} \tag{15}$$

Substituting the right-hand side of Equation (7) for p_2 in Equation (15) results in

$$T_2 = \left(\frac{p_{hp}}{p_{atm}}\right)^{\gamma-1} T_{atm} \tag{16}$$

Substituting the right-hand side of Equation (16) for T_2 in Equation (13) results in

$$\begin{aligned} _2q_3 &= c_v\left(T_{atm} - \left(\frac{p_{hp}}{p_{atm}}\right)^{\gamma-1} T_{atm}\right) \\ &= c_v T_{atm}\left(1 - \left(\frac{p_{hp}}{p_{atm}}\right)^{\gamma-1}\right) \end{aligned} \tag{17}$$

Unlike the post-compression heat transfer, which occurs as a constant-volume process, the post-expansion heat transfer, heat absorption from V_4 to V_1 ,takes place at constant pressure. Thus,

$$ {}_4q_1 = c_p\left(T_1 - T_4\right) = c_p\left(T_{atm} - T_4\right) \tag{18} $$

As with T_2, T_4 can be written in terms of pressure by using the isentropic pressure-temperature relationship, applied between states 3 and 4:

$$ \frac{p_3}{p_4} = \left(\frac{T_3}{T_4}\right)^{\frac{\gamma}{\gamma-1}} \rightarrow \frac{p_{hp}}{p_{atm}} = \left(\frac{T_{atm}}{T_4}\right)^{\frac{\gamma}{\gamma-1}} \tag{19} $$

Solving Equation (19) for T_4:

$$ T_4 = \left(\frac{p_{atm}}{p_{hp}}\right)^{\frac{\gamma-1}{\gamma}} T_{atm} \tag{20} $$

Substituting the right-hand side of Equation (20) for T_4 in Equation (18) results in

$$ {}_4q_1 = c_p\left(T_{atm} - \left(\frac{p_{atm}}{p_{hp}}\right)^{\frac{\gamma-1}{\gamma}} T_{atm}\right) $$

$$ = c_p T_{atm}\left(1 - \left(\frac{p_{hp}}{p_{atm}}\right)^{\frac{1-\gamma}{\gamma}}\right) \tag{21} $$

B. ISOTHERMAL CYCLE ANALYSIS

Unlike the isentropic cycle, the work and heat transfer processes for the isothermal CAES cycle cannot be separated because the heat generated by compression and lost by expansion is assumed to be transferred to and from the atmosphere instantaneously. Therefore, whereas pressure in the isentropic cycle rises due to changes in both system volume and system temperature, heat transfer assumption for the isothermal cycle results in system pressure rising due to the change in system volume only. Consequently, the isothermal cycle is the most efficient model for a CAES system. Figure 16 shows how the isothermal work processes relate to each other

thermodynamically. Of note, state 2t in the isothermal cycle is the same as state 3 in the isentropic cycle. Figures 17 and 18 illustrate the isothermal compression and expansion phases, respectively, and the resultant states:

- State 1 (dotted-line control mass of Figures 17 and 18) describes the air at atmospheric pressure and temperature, p_{atm} and T_{atm}, respectively, within an initial volume, V_1, both before isothermal compression and after isothermal expansion.
- State 2t (dashed-line control mass of Figures 17 and 18) describes the air at T_{atm} and the desired high pressure, p_{hp}, both after isothermal compression and before isothermal expansion.

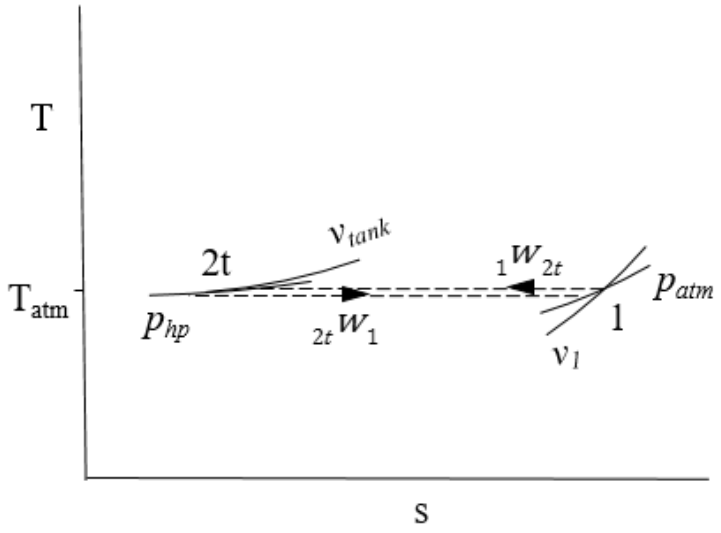

Figure 16. Temperature-Entropy Diagram for Isothermal CAES System Cycle

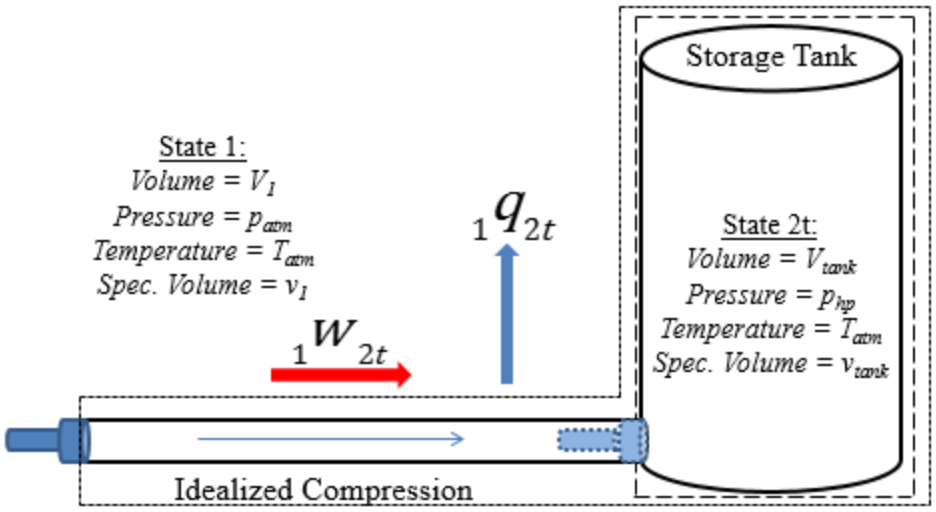

Figure 17. System Diagram Showing Processes and States for Isothermal Compression Phase.

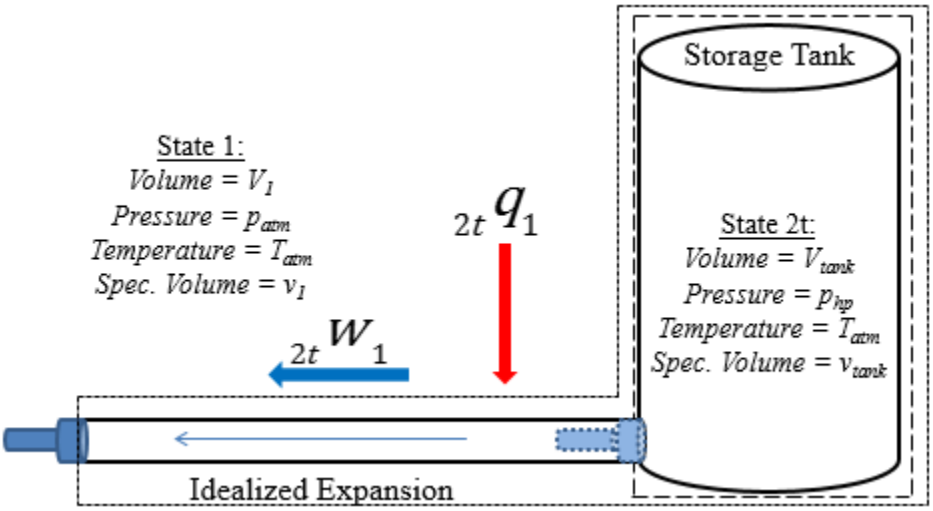

Figure 18. System Diagram Showing Processes and States for Isothermal Expansion Phase.

Figure 16 shows that the pressure at state 2 is p_{hp}. This is proven by Equation (22).

$$p_{2t} = p_{atm}\left(\frac{v_1}{v_{tank}}\right) = p_{atm}\left(\frac{p_{hp}}{p_{atm}}\right) = p_{hp} \tag{22}$$

The isothermal pressure-volume relationship shown in Equation (22) results in isothermal compression specific work being calculated as

$$
\begin{aligned}
{}_1w_{2t} &= \int_1^{2t} pdv = p_1 v_1 \ln \frac{v_{tank}}{v_1} \\
&= R_{air} T_{atm} \ln \frac{p_{atm}}{p_{hp}}
\end{aligned}
\tag{23}
$$

The isothermal expansion specific work process is calculated in much the same way, since $p_{hp} v_{tank} = p_1 v_1$. Thus,

$$
\begin{aligned}
{}_{2t}w_1 &= p_1 v_1 \ln \frac{v_1}{v_{tank}} \\
&= R_{air} T_{atm} \ln \frac{p_{hp}}{p_{atm}}
\end{aligned}
\tag{24}
$$

and thus, as expected,

$$
{}_{2t}w_1 = -{}_1w_{2t} \tag{25}
$$

Using Equation (1) as the definition for isothermal cycle efficiency reveals that this cycle is 100% efficient; this is a direct result of the previously discussed instantaneous heat transfer assumption. The specific heat transfer to and from the atmosphere for these isothermal processes, illustrated in Figures 17 and 18, respectively, cannot be found using Equation (13) due to a lack of temperature difference; instead, the enthalpy form of the Gibbs equation for a change in entropy of an ideal gas must be used. Equation (26) shows the formula applied to the isothermal compression process:

$$
s_{2t} - s_1 = \frac{{}_1q_{2t}}{T_1} = c_p \ln\left(\frac{T_1}{T_{2t}}\right) - R_{air} \ln\left(\frac{p_{2t}}{p_1}\right) \tag{26}
$$

A derivation of this formula can be found in *Fundamental of Thermodynamics*, by Borgnakke and Sonntag [54]. Solving Equation (26) for ${}_1q_{2t}$:

$$
\begin{aligned}
{}_1q_{2t} &= -T_1 R_{air} \ln\left(\frac{p_{2t}}{p_1}\right) \\
&= -T_{atm} R_{air} \ln\left(\frac{p_{hp}}{p_{atm}}\right)
\end{aligned} \tag{27}
$$

As with the relationship between isothermal specific compression and expansion work processes shown by Equation (25), the specific heat transfer for isothermal expansion is equal in magnitude and opposite in sign to the specific heat transfer for isothermal compression.

C. EFFECTS OF THERMAL ENERGY STORAGE

Figure 19 shows the relationships between isentropic and isothermal specific work processes based on p_{hp}: ${}_1w_2$ requires exponentially more energy than ${}_1w_{2t}$, and likewise for ${}_2w_1$ compared to ${}_{2t}w_1$. Also shown is the effect that TES has on CAES systems: any amount of thermal energy captured during the compression process results in the compressor requiring less energy for a given operating pressure and any amount of thermal energy transferred to the air during expansion allows the expansion device to extract more energy for a given operating pressure. Overall, the system's operational characteristic approaches that of the isothermal process, and cycle efficiency improves.

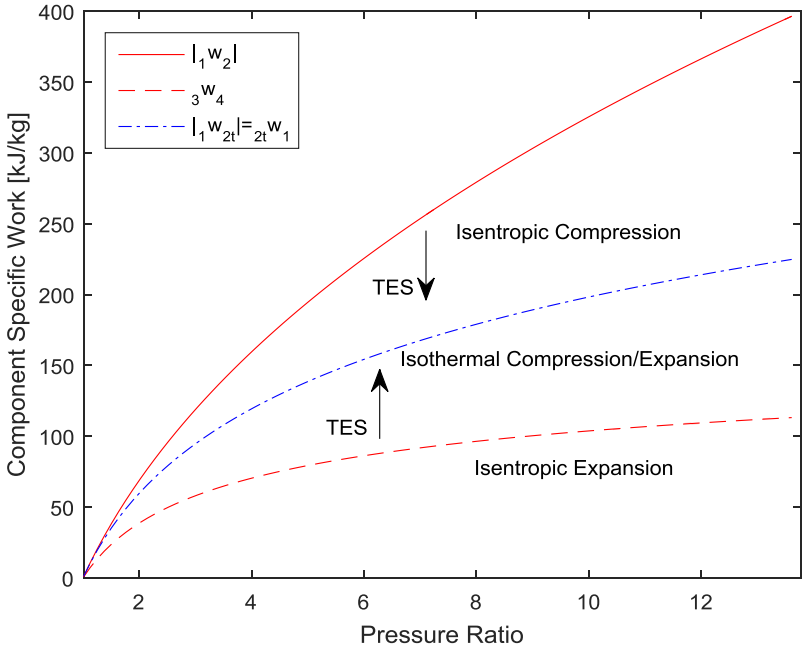

Figure 19. Component Specific Work Based on Final System Pressure.

D. POWER ANALYSIS

The compression phase of this system was also analyzed for both total power and specific power, specific power being defined as the power per unit mass flow rate. The control-mass assumption for this system required the mass flow rate to be defined as the mass of air entering the tank volume per second. Thus

$$\dot{m} \equiv \rho(t)Q \tag{28}$$

where Q is the piston's volumetric rate of change, which was initially assumed constant.

1. Isentropic Compression

Determining isentropic compression power requires a derivative of the work formula with respect to time. To apply the derivative, the isentropic compression work formula can be written as a function of time as

$$W_s(t) = \frac{1}{1-\gamma}\left(p_s(t)V(t) - p_1V_1\right) \tag{29}$$

where $p_1 = p_{atm}$ and V_1 is the initial system volume based on the desired system operating pressure. Based on Equation (29), the isentropic power formula is written as

$$\dot{W}_s(t) = \frac{dW_s(t)}{dt} = \frac{1}{1-\gamma}\frac{d}{dt}\left[p_s(t)V(t) - p_{atm}V_1\right] = \frac{1}{1-\gamma}\frac{d}{dt}\left[p_s(t)V(t)\right] \tag{30}$$

Because both pressure and volume change with time in Equation (30), the Product Rule for derivatives must be applied to the pressure-volume product as

$$\frac{d}{dt}\left[p_s(t)V(t)\right] = \frac{dp_s(t)}{dt}V(t) + p_s(t)\frac{dV(t)}{dt} \tag{31}$$

To evaluate Equation (31) the individual components must be determined. System volume over time, $V(t)$, starts at V_1 and, assuming a limitless supply of power, decreases linearly over time due to the compressor's constant volumetric flow rate, Q. Thus,

$$V(t) = V_1 - Qt \tag{32}$$

and it follows that

$$\frac{dV(t)}{dt} = -Q \tag{33}$$

System pressure as a function of time, $p(t)$, is determined by rearranging Equation (2) as

$$p_s(t) = \frac{constant}{V(t)^\gamma} = \frac{p_{atm}V_1^\gamma}{(V_1 - Qt)^\gamma} \tag{34}$$

The derivative for Equation (34) can be found using both the Quotient Rule and the Chain Rule for derivatives. Thus

$$\frac{dp_s(t)}{dt} = \frac{(V_1 - Qt)^{\gamma}(0) - p_{atm}V_1^{\gamma}\left[\gamma(V_1 - Qt)^{\gamma-1}(-Q)\right]}{(V_1 - Qt)^{2\gamma}}$$

which, after simplification, becomes

$$\frac{dp_s(t)}{dt} = \frac{p_{atm}V_1 Q\gamma\left(\frac{V_1}{V_1 - Qt}\right)^{\gamma-1}}{(V_1 - Qt)^2} \tag{35}$$

Putting Equations (32) through (35) back into Equation (30) results in

$$\begin{aligned}
\dot{W}_s(t) &= \frac{1}{1-\gamma}\left[\frac{p_{atm}V_1 Q\gamma\left(\frac{V_1}{V_1 - Qt}\right)^{\gamma-1}}{\left(V_1 - Qt\right)^2}\left(V_1 - Qt\right) + \frac{p_{atm}V_1^{\gamma}}{\left(V_1 - Qt\right)^{\gamma}}\left(-Q\right)\right] \\
&= \frac{1}{1-\gamma}\left[\frac{p_{atm}V_1 Q\gamma\left(\frac{V_1}{V_1 - Qt}\right)^{\gamma-1}}{\left(V_1 - Qt\right)} - p_{atm}Q\left(\frac{V_1}{V_1 - Qt}\right)^{\gamma}\right] \\
&= \frac{1}{1-\gamma}p_{atm}Q\left(\frac{V_1}{V_1 - Qt}\right)^{\gamma}\left[\gamma - 1\right] = \frac{\gamma - 1}{1-\gamma}p_{atm}Q\left(\frac{V_1}{V_1 - Qt}\right)^{\gamma} \\
&= -Qp_{atm}\left(\frac{V_1}{V_1 - Qt}\right)^{\gamma} \\
&= -Qp_s(t)
\end{aligned} \tag{36}$$

and therefore isentropic compression power is directly proportional to the isentropic system pressure. This relationship can be seen by the similar shapes of isentropic power and pressure in Figures 20 and 21 in the following section.

As previously stated, specific power was defined as power per unit mass flow rate. Thus, for isentropic compression, Equations (28) and (36) were combined to calculate specific power as

$$\dot{w}_s(t) = \frac{\dot{W}_s(t)}{\dot{m}} = \frac{-Qp_s(t)}{\rho_s(t)Q} = \frac{-p_s(t)}{\rho_s(t)} \tag{37}$$

The density function in Equation (37) can be calculated using the Ideal Gas Law:

$$\rho_s(t) = \frac{p_s(t)}{R_{air}T_s(t)} \tag{38}$$

The temperature function in Equation (38) can be calculated by writing the isentropic pressure-temperature relationship in Equation (14) as a function of time:

$$\frac{p_{atm}}{p_s(t)} = \left(\frac{T_{atm}}{T_s(t)}\right)^{\frac{\gamma}{\gamma-1}} \tag{39}$$

The time-dependent temperature variable in Equation (39) is solved as

$$T_s(t) = T_{atm}\left(\frac{p_s(t)}{p_{atm}}\right)^{\frac{\gamma-1}{\gamma}} \tag{40}$$

Substituting the right-hand side of Equation (40) for $T_s(t)$ in Equation (38) results in

$$\rho_s(t) = \frac{p_s(t)}{R_{air}T_{atm}\left(\frac{p_s(t)}{p_{atm}}\right)^{\frac{\gamma-1}{\gamma}}} = \frac{p_s(t)\left(\frac{p_{atm}}{p_s(t)}\right)^{\frac{\gamma-1}{\gamma}}}{R_{air}T_{atm}} = \frac{p_s(t)p_s(t)^{\frac{1-\gamma}{\gamma}}p_{atm}^{\frac{\gamma-1}{\gamma}}}{R_{air}T_{atm}}$$

$$= \frac{p_s(t)^{\frac{1}{\gamma}}p_{atm}^{\frac{\gamma-1}{\gamma}}}{R_{air}T_{atm}} \tag{41}$$

Substituting the right-hand side of Equation (41) for $\rho_s(t)$ in Equation (37) results in

$$\dot{w}_s(t) = \frac{-p_s(t)}{\rho_s(t)} = \frac{-p_s(t)}{\frac{p_s(t)^{\frac{1}{\gamma}} p_{atm}^{\frac{\gamma-1}{\gamma}}}{R_{air}T_{atm}}} = \frac{-R_{air}T_{atm}p_s(t)p_s(t)^{-\frac{1}{\gamma}}}{p_{atm}^{\frac{\gamma-1}{\gamma}}} = \frac{-R_{air}T_{atm}p_s(t)^{\frac{\gamma-1}{\gamma}}}{p_{atm}^{\frac{\gamma-1}{\gamma}}}$$

$$= -R_{air}T_{atm}\left(\frac{p_s(t)}{p_{atm}}\right)^{\frac{\gamma-1}{\gamma}} \tag{42}$$

2. Isothermal Reference

Isothermal compression power can be determined in the same manner as for the isentropic compression process, with the isothermal work formula written as a function of time as

$$W_{th}(t) = p_{th}(t)V(t)\ln\frac{V(t)}{V_1} \tag{43}$$

or

$$W_{th}(t) = p_{atm}V_1\ln\frac{V(t)}{V_1} \tag{44}$$

since $pV = constant$ for the isothermal work process. Given that Equation (44) contains only one variable that changes with time, the power calculation evaluates as

$$\begin{aligned}\dot{W}_{th}(t) &= \frac{dW_{th}(t)}{dt} = \frac{d}{dt}\left[p_{atm}V_1\ln\frac{V(t)}{V_1}\right] = p_{atm}V_1\frac{d}{dt}\left[\ln\frac{V(t)}{V_1}\right] \\ &= p_{atm}V_1\frac{d}{dt}\left[\ln V(t) - \ln V_1\right] = p_{atm}V_1\frac{d}{dt}\left[\ln\left(V_1 - Qt\right) - \ln V_1\right] \\ &= -Qp_{atm}\frac{V_1}{V_1 - Qt} \\ &= -Qp_{th}(t)\end{aligned} \tag{45}$$

and therefore, just as with the isentropic compression process, isothermal compression power is directly proportional to the isothermal system pressure. This relationship is also shown when comparing Figures 20 and 21. Finally, due to the exponential aspect of the isentropic pressure-volume relationship compared to the linear aspect of the isothermal pressure-volume relationship, Figure 20 shows that the isentropic compression process requires exponentially more power than the isothermal compression process as the system pressure rises over time.

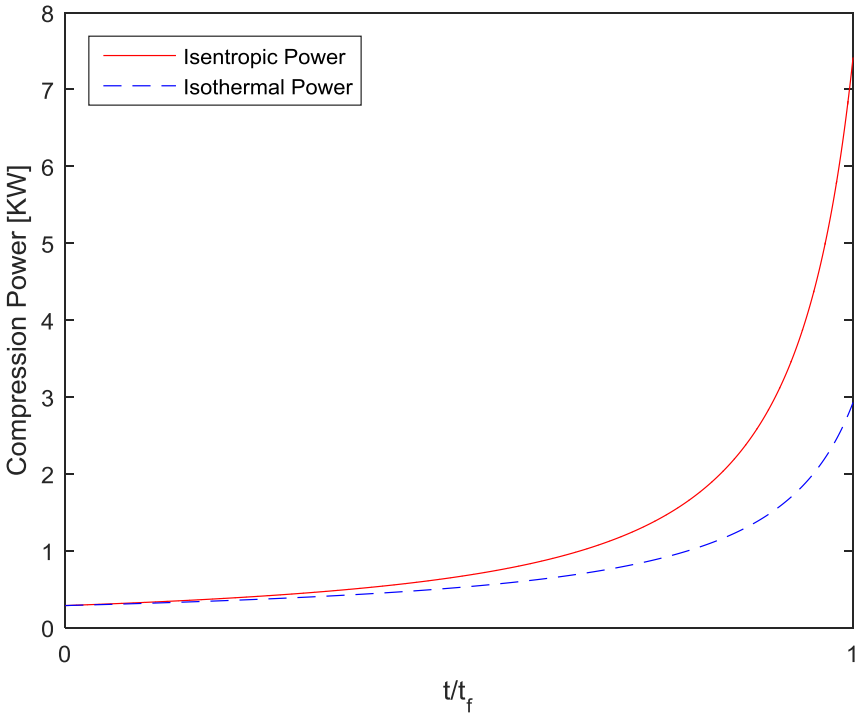

Figure 20. Magnitudes of Isentropic and Isothermal Power, Normalized to Charging Time for 10.34 Bar (150 psi).

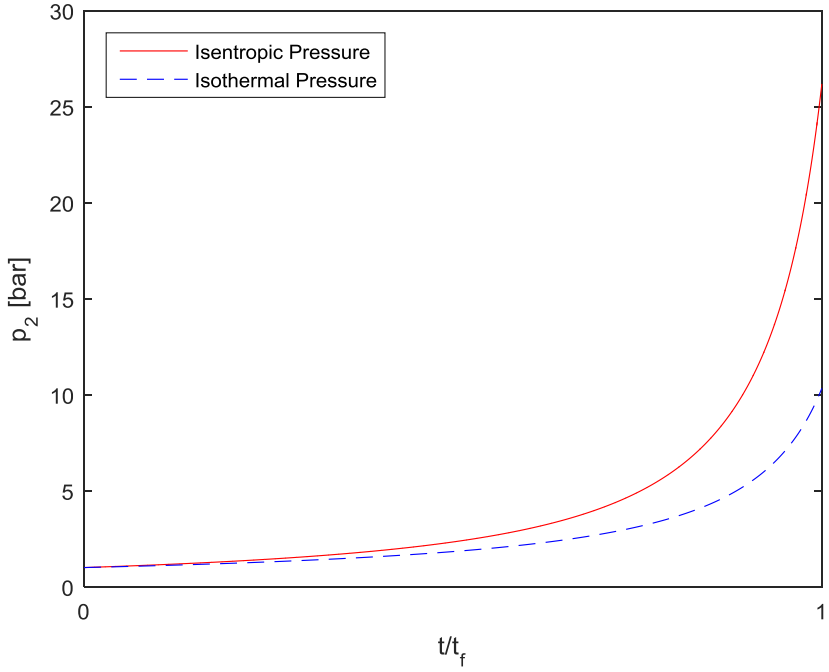

Figure 21. Magnitudes of Isentropic and Isothermal Pressure, Normalized to Charging Time for 10.34 Bar (150 psi).

In regards to isothermal specific power, Equation (37) is applied to the isothermal process as

$$\dot{w}_{th}(t) = \frac{\dot{W}_{th}(t)}{\dot{m}} = \frac{-Qp_{th}(t)}{\rho_{th}(t)Q} = \frac{-p_{th}(t)}{\rho_{th}(t)} \tag{46}$$

Again, the density function is determined using the Ideal Gas Law:

$$\rho_{th}(t) = \frac{p_{th}(t)}{R_{air}T_{th}(t)} = \frac{p_{th}(t)}{R_{air}T_{atm}} \tag{47}$$

Substituting the right-hand side of Equation (47) for $\rho_{th}(t)$ in Equation (46) results in

$$\dot{w}_{th}(t) = \frac{-p_{th}(t)}{\rho_{th}(t)} = \frac{-p_{th}(t)}{\frac{p_{th}(t)}{R_{air}T_{atm}}}$$
$$= -R_{air}T_{atm} \tag{48}$$

Equation (48) shows that the power per unit mass flow rate remains constant during the isothermal compression process. The relationship between isentropic and isothermal specific compression power is illustrated in Figure 22.

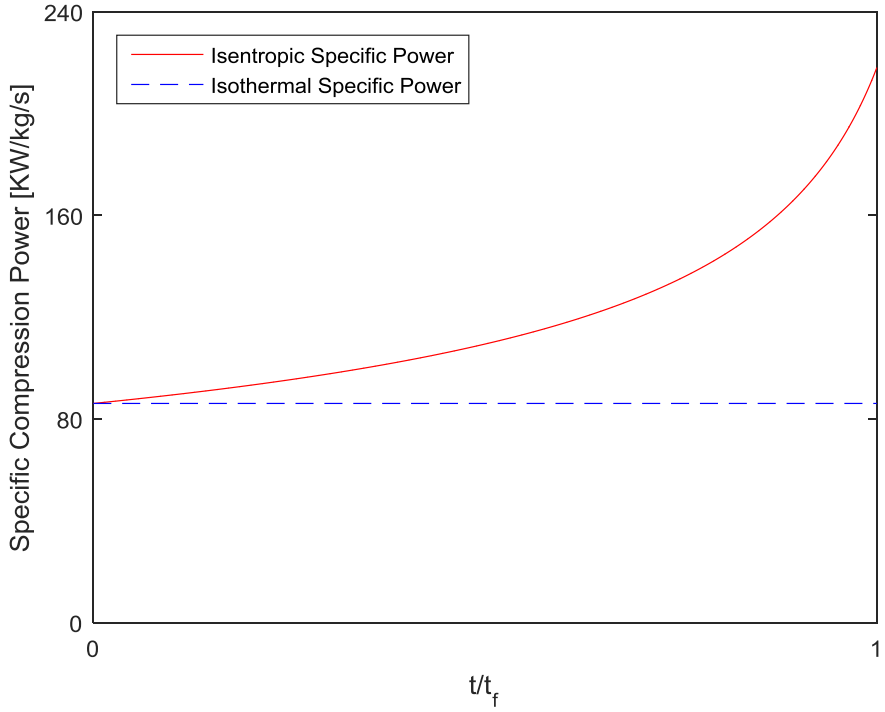

Figure 22. Magnitudes of Isentropic and Isothermal Specific Power, Normalized to Charging Time for 10.34 Bar (150 psi).

3. Compressor Power Limitation

As mentioned earlier, the previous power consumption calculations assumed a limitless power supply. To apply the effect of a capped power supply, the compressor's flowrate, Q, is reduced when the power consumption value reaches the power supply

limit (3 kW for this particular SS-CAES). Figures 23 and 24 show pressure rise and nominal flowrate percentage respectively over time for both the isentropic and isothermal process when the allowed power consumption value is limited to the power supply. This figure shows that when system pressure has reached the point where power consumption equals power supply, the mathematical relationship of flowrate and pressure in Equations (36) and (45) requires that flowrate decrease exponentially to allow pressure to rise while keeping power constant. In comparison to the isothermal pressure rise, the isentropic pressure rise gets limited earlier due to the exponential rise in pressure—and thus power—with respect to time. This limited pressure rise results in the flowrate for the isentropic process being reduced to 40% of its original value by the time system pressure reaches 10.34 bar (150 psi), whereas the isothermal process retains its original flowrate. Overall, the isentropic process would require over twice as much time as the isothermal process due to exponential pressure rise.

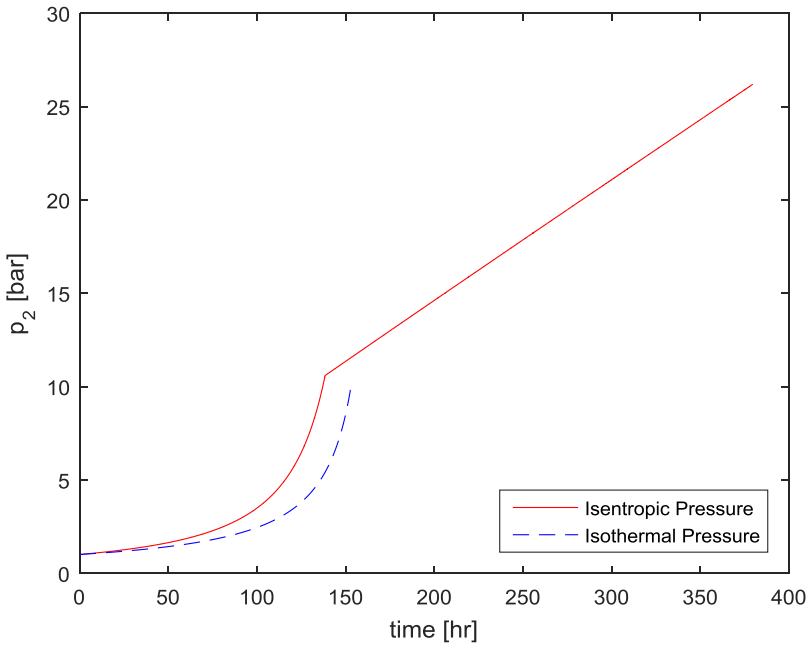

Figure 23. Pressure Over Time for a Capped Power Supply.

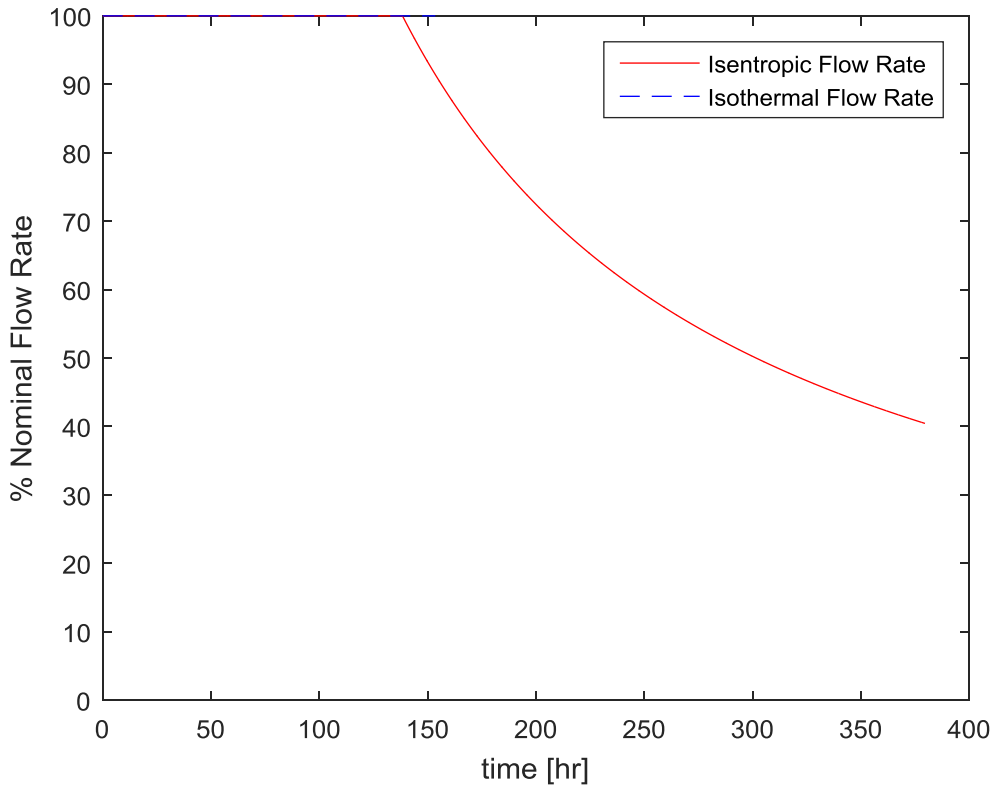

Figure 24. Nominal Flow Rate Percentage Over Time for a Capped Power Supply.

III. SYSTEM CONFIGURATION

A. DESIGN CONSIDERATIONS

The initial goal of this project was to augment the IMPREL's aging, energy *inefficient* air compressor system—comprised of a 450 kW 3-stage centrifugal compressor followed by a 112 kW piston-cylinder boost compressor that together pressurize supersonic wind tunnel storage tanks—with a system completely powered by solar energy. The design criteria in Table 2 were established to accommodate the available power supply as well as thermodynamic requirements of the supersonic wind tunnel.

Table 2. Compression System Design Criteria.

Parameter	Quantity	Criterion
Compressor input power	3 kW, single-phase AC	PV array maximum output
Compressor discharge pressure	2 MPa (290 psia)	Supersonic wind tunnel supply pressure
Air Dryer dew point	-40 °C (-40 °F)	Prevent wind tunnel damage from condensation of humidity

Reaching the desired discharge pressure with the given power supply proved unachievable when local compressor companies informed the author that the power supply limitation restricted compressor discharge pressure to 1.2 MPa (175 psi). With this additional restriction in hand, the project's goal was updated to install a compressor that would augment the centrifugal compressor. The system components are illustrated in Figure 25 and their functions are described in the following sections.

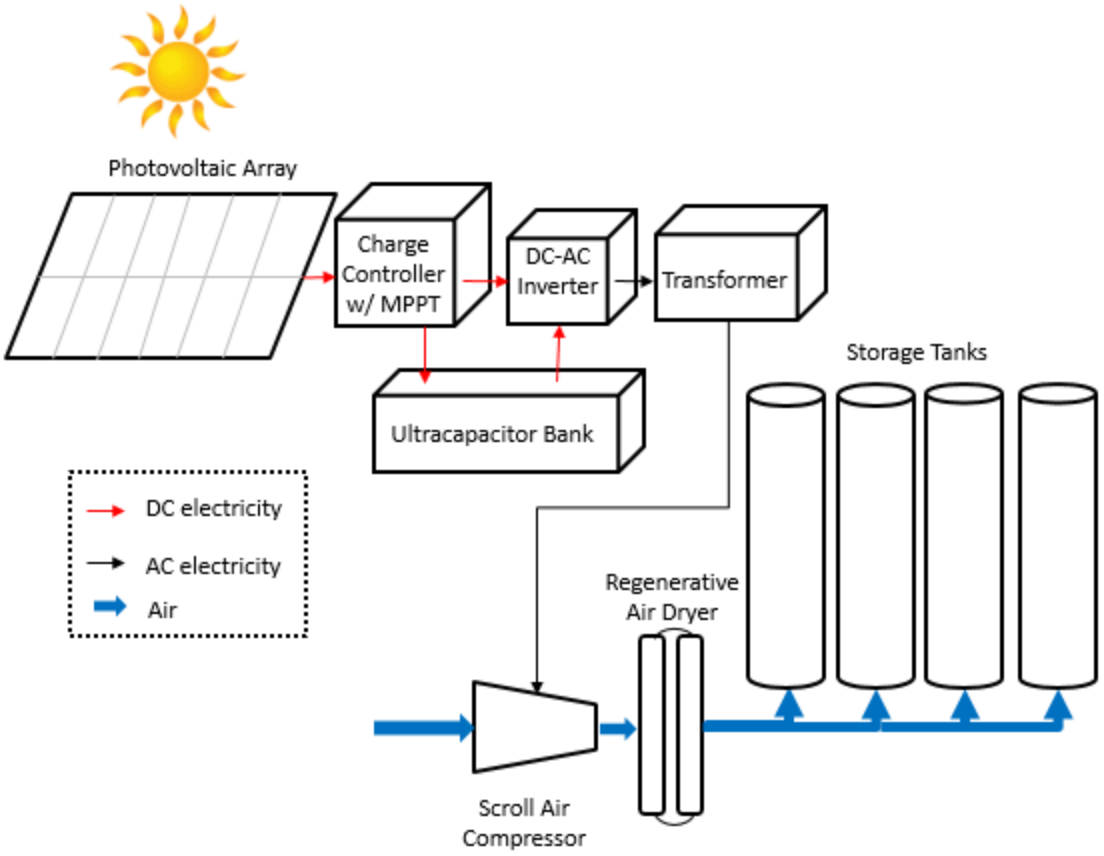

Figure 25. One-Line Diagram for Supply Side of Solar-Powered, Small-Scale CAES.

B. SOLAR-POWERED MICRO GRID

The micro grid that powers the compressed air system consists of a PV array, ultracapacitors, a maximum power point tracking (MPPT) controller, and a DC-to-AC inverter. Figure 26 shows the electrical flow paths for this micro grid and the following paragraphs describe the operation of each component.

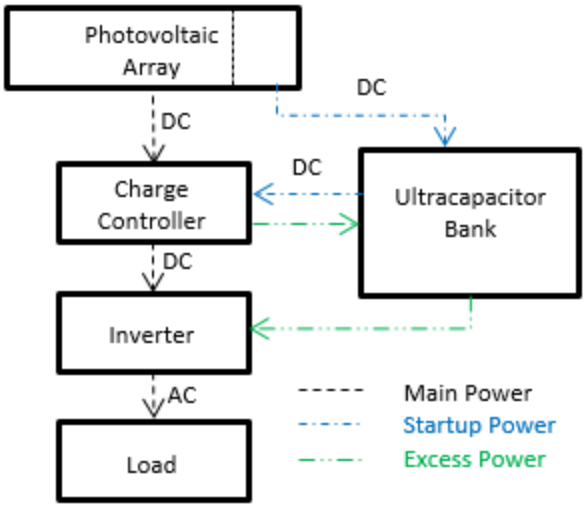

Figure 26. One-Line Electrical Diagram of Solar-Powered Micro Grid.

1. Normal Operations

Solar radiance is converted to electrical energy by a PV array comprised of 12 300 W panels, shown in Figure 27. Ten panels of the array provide a nominal 3 kW for system loading. A MidNite Solar Classic 150 MPPT charge controller, shown in Figure 28, optimizes the PV array's variable DC voltage output. Figure 29 illustrates that by continuously maximizing the PV array's power output, the MPPT circuit also maximizes available loading amperage [55]. Following this process, a SMA Sunny Island invertor, shown in Figure 28, converts the electrical current from DC to AC and sends power to the load.

Figure 27. Fixed-Axis PV Array Outside Integrated Multi-Physics Renewable Energy Lab.

Figure 28. SMA Sunny Island Inverter (Yellow) and MidNite Solar Charge Controller (Black).

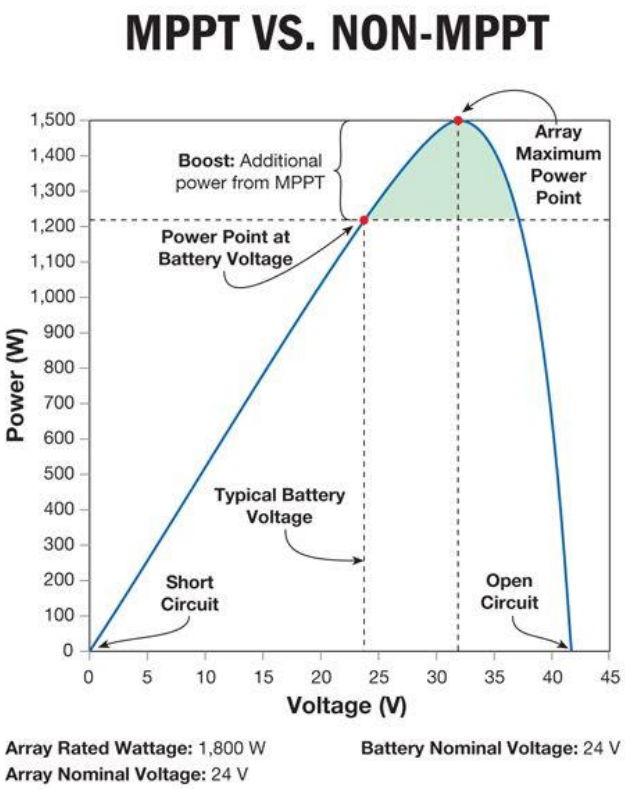

Figure 29. Maximum Power Point Tracking Graph of Typical Charge Controller. Source: [55].

2. Startup Power and Excess Storage

Startup power is supplied by—and excess energy storage is stored in—a bank of Maxwell 130F ultracapacitors, an example of which is shown in Figure 30. As indicated by Figure 26, portion of the PV array (two panels) charge the ultracapacitor bank until voltage builds up to provide startup power to the MidNite Solar charge controller. After the charge controller starts, it uses MPPT to fully charge the ultracapacitor bank with the remaining 10 PV panels. Following this startup operation, the ultracapacitors store surplus energy (Up to 56.6 Wh per capacitor) when the PV array is producing power in excess of load requirements.

Figure 30. Maxwell 130F Ultracapacitor. Source: [56].

C. COMPRESSION SYSTEM

1. Rotary Compressor

Based on runtime require to achieve desired system pressure, a rotary compressor was chosen over a reciprocating compressor. A rotary compressor has a smoother operation and its compression method, illustrated in Figure 31 as air being compressed by a gradually-reduced cavity [57], allows for a more durable construction. The specific compressor is a 2-H.P. Powerex Oil-less Scroll air compressor; Figure 32 shows its setup integrated with a 60-gal holding tank.

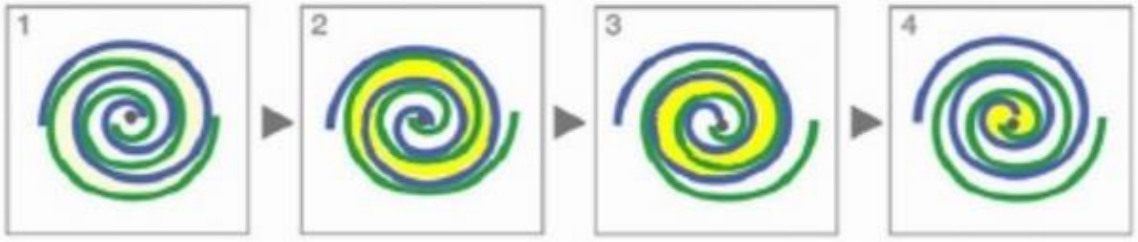

Figure 31. Principle of Operation for a Powerex Oil-less Scroll Air Compressor. Source: [57].

Figure 32. Powerex Oil-less Scroll Air Compressor. Source: [57].

1. Air Dryer

This system's air dryer, a regenerative dual-tower shown in Figure 33, removes humidity from the air via a regenerative desiccant drying process (described in Figure 34). This type of air dryer protects the wind tunnel from the destructive effects of entrained humidity and avoids any hazardous material concerns encountered in other air dryer technologies.

Figure 33. Zander Ecodry Series Desiccant Dryer. Source: [58].

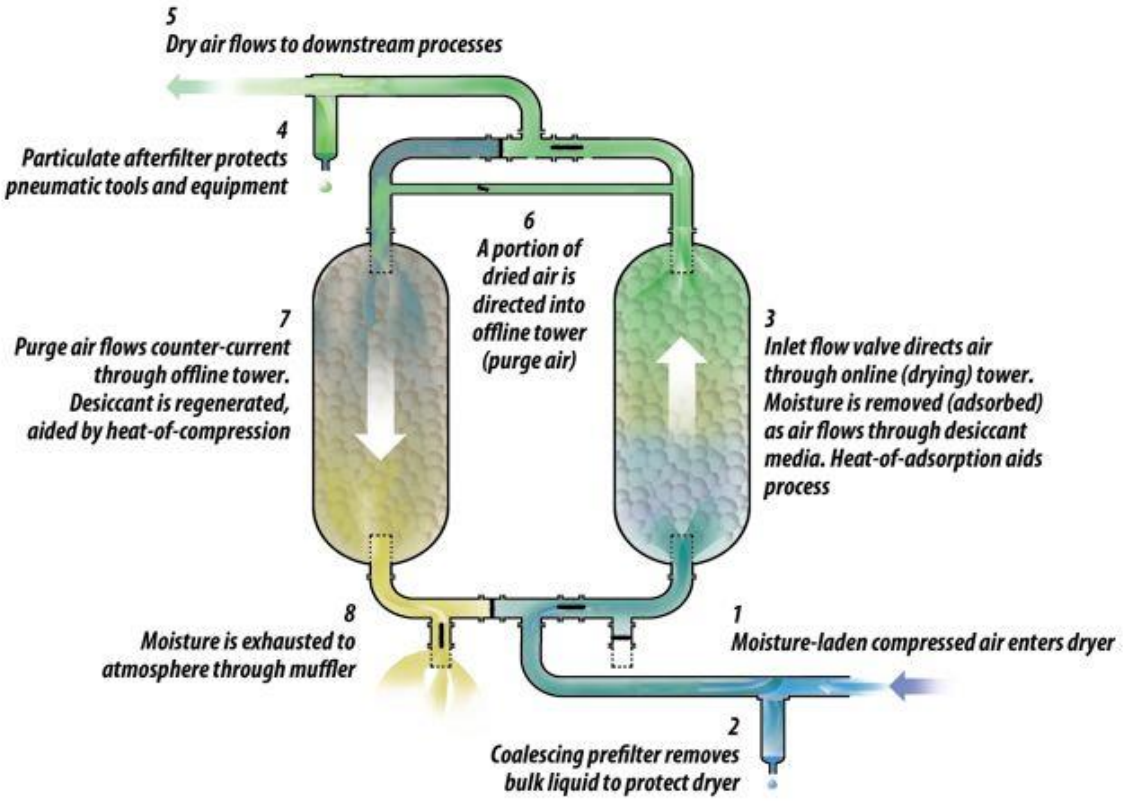

Figure 34. Operational Description of a Dual Tower, Heatless, Regenerative Desiccant Air Dryer. Source: [59].

2. Storage Tanks

As previously stated at the beginning of this chapter, this system will replace a portion of the compression system that is used to charge a supersonic wind tunnel. Because supersonic wind tunnels require an immense mass of air for even relatively short periods of operations, the tanks being used for this SS-CAES, shown in Figure 35, are oversized but were already in place at IMPREL.

Figure 35. Air Storage Tanks.

THIS PAGE INTENTIONALLY LEFT BLANK

IV. CONCLUSIONS AND RECOMMENDATIONS

The analysis portion of this study showed how fundamental principles of thermodynamics could be used to develop a control mass approach for CAES systems. This approach resulted in an isentropic CAES system cycle efficiency that is succinctly described in terms of the system's pressure ratio. The comparison of isentropic and isothermal cycles showed how TES implementation can directly improve system efficiency. Furthermore, the power formulas derived using this approach can easily be used to both size the compressor based on power supply limitations and estimate system charging time.

The final design of this compression system, when installed, will use clean energy to augment nearly 50% of the current supersonic wind tunnel compression system's energy use, and it will keep the tunnel at a higher state of readiness.

Recommendations for future study:

- After system has been verified operational, design control strategy that ensures compressor is operating at maximum efficiency with respect to solar power input.
- Integrate compression system with an expansion system recently developed by Mclaughlin [52] to demonstrate and collect data on a proof-of-concept solar-powered SS-CAES system.
- Design a TES system that harnesses compression heat for use during the expansion phase and does so via phase change material.

THIS PAGE INTENTIONALLY LEFT BLANK

APPENDIX A. EQUATION SUMMARY

$$ {}_1w_2 = R_{air} T_{atm} \frac{1}{(1-\gamma)} \left(\left(\frac{p_{hp}}{p_{atm}} \right)^{\gamma-1} - 1 \right) $$

$$ {}_2q_3 = c_v T_{atm} \left(1 - \left(\frac{p_{hp}}{p_{atm}} \right)^{\gamma-1} \right) $$

$$ {}_3w_4 = R_{air} T_{atm} \frac{1}{(1-\gamma)} \left(\left(\frac{p_{atm}}{p_{hp}} \right)^{\frac{\gamma-1}{\gamma}} - 1 \right) $$

$$ {}_4q_1 = c_p T_{atm} \left(1 - \left(\frac{p_{hp}}{p_{atm}} \right)^{\frac{1-\gamma}{\gamma}} \right) $$

$$ \eta = \frac{{}_3w_4}{{}_1w_2} = \left| \frac{\left(\left(\frac{p_{atm}}{p_{hp}} \right)^{\frac{\gamma-1}{\gamma}} - 1 \right)}{\left(\left(\frac{p_{atm}}{p_{hp}} \right)^{1-\gamma} - 1 \right)} \right| $$

$$ {}_1w_{2t} = R_{air} T_{atm} \ln \frac{p_{atm}}{p_{hp}} $$

$$ {}_1q_{2t} = -T_{atm} R_{air} \ln \left(\frac{p_{hp}}{p_{atm}} \right) $$

$$ {}_{2t}w_1 = R_{air} T_{atm} \ln \frac{p_{hp}}{p_{atm}} $$

$$ \dot{W}(t) = -Qp(t) $$

$$ \dot{w}_s(t) = \frac{-p_s(t)}{\rho(t)} = -R_{air} T_{atm} \left(\frac{p_s(t)}{p_{atm}} \right)^{\frac{\gamma-1}{\gamma}} $$

$$ \dot{w}_{th}(t) = \frac{-p_{th}(t)}{\rho(t)} = -R_{air} T_{atm} \left(\frac{p_{th}(t)}{p_{atm}} \right)^{\frac{\gamma-1}{\gamma}} $$

APPENDIX B. MATLAB CODE

```
%% Thomas Prinsen/Thesis/CAES System Cycle & Power Analysis

clc
clear all

%% Constants
Tatm = 300;   %Atm temperature [K]
Patm = 101325;  %Atm pressure [Pa]
Vtank = 170;   %Tank volume [m^3]
n = 1.4;    %Polytropic index
R_air = 287.058;  %Air gas constant [J/kg-K]
Cv = 718;    %Air const. vol. spec. heat [J/kg-K]
Q = 0.0028317;   %Supply volumetric flow rate [m^3/s]
pwrmax = 3;   %Max compressor supply power [KW]

%% Initializing Data Matrices
P_hp = linspace(101326,1378952)';
          %desired system high pressure (14.7-200 psia)
PR = P_hp/Patm;     %system pressure ratio
m = zeros(100,1);    %System mass [kg]
V1 = zeros(100,1);    %Initial volume [m^3]
P2_isent = zeros(100,1);  %Max system pressure, post-isentropic
compression
P2_isoth = zeros(100,1);  %Max system pressure, post-isothermal
compression
T2 = zeros(100,1);    %Max system temperature
V4 = zeros(100,1);    %System volume, post-isentropic expansion
work_comp_isentropic = zeros(100,1);
          %specific work of isentropic compression
work_comp_isothermal = zeros(100,1);
          %specific work of isothermal compression
work_turb_isentropic = zeros(100,1);
          %specific work of isentropic expansion
work_turb_isothermal = zeros(100,1);
          %specific work of isothermal expansion
CycleEff = zeros(100,1);  %Cycle thermal efficiency
q_23 = zeros(100,1);   %specific heat transfer after isentropic comp
q_12t = zeros(100,1);   %specific heat transfer during isothermal comp

%% Calculations for Energy, Efficiency
for i = 1:100

  %**COMPRESSION STAGE**
  %mass of air needed
  m(i) = P_hp(i)*Vtank/(R_air*Tatm);
  %Initial volume needed (at Patm and Tatm)
  V1(i) = m(i)*R_air*Tatm/Patm;
  %Pressure the tank will need to be pumped up for isentropic
compression
  % to before heat loss (State 2)
```

```
  P2_isent(i) = Patm*(V1(i)/Vtank)^n;
  %Pressure the tank will need to be pumped up for isothermal
compression
  % to before heat loss (State 2)
  P2_isoth(i) = Patm*(V1(i)/Vtank);
  %Max temp of tank before heat loss
  T2(i) = (P2_isent(i)/P_hp(i))*Tatm;
  %Isentropic compressor specific work [kJ/kg]
  work_comp_isentropic(i) = abs((1/(1-n))*...
   (P2_isent(i)*Vtank - Patm*V1(i)))/(m(i)*1000);
  %Isothermal compressor specific work (ideal reference) [kJ/kg]
  work_comp_isothermal(i) =
abs(Patm*V1(i)*log(Vtank/V1(i)))/(m(i)*1000);

  %**EXPANSION STAGE**
  %Pressure the tank will expand to before heat gain from atmosphere
  % (State 4)
  V4(i) = ((P_hp(i)/Patm)*Vtank^n)^(1/n);
  %Isentropic turbine specific work [kJ/kg]
  work_turb_isentropic(i) = (1/(1-n))*...
   (Patm*V4(i)-P_hp(i)*Vtank)/(m(i)*1000);
  %Isothermal turbine specific work (ideal reference) [kJ/kg]
  work_turb_isothermal(i) =
(P_hp(i)*Vtank*log(V1(i)/Vtank))/(m(i)*1000);

  %**CYCLE EFFICIENCY** ratio of work output to work input
  CycleEff(i) = (work_turb_isentropic(i)/work_comp_isentropic(i))*100;

end

%Convert pascal to bar for graphing
Psys_bar  = P_hp/100000;
P2_isent_bar = P2_isent/100000;
P2_isoth_bar = P2_isoth/100000;

%Graphing Compressor and Turbine Work, Cycle Efficiency
figure %isentropic compression vs isothermal compression
plot(PR,work_comp_isentropic,'r'), hold on
plot(PR,work_comp_isothermal,'b--')
xlim([1.015 13.78])
xlabel 'Pressure Ratio'
ylabel 'Compression Specific Work [kJ/kg]';
legend('Isentropic','Isothermal','Location','NW')
annotation('textbox',...
  [0.43035714285714 0.338095238095242 0.278571428571429
0.0619047619047649],...
  'String','Isothermal Compression',...
  'FitBoxToText','off',...
  'EdgeColor',[1 1 1]);
annotation('textbox',...
  [0.576785714285714 0.626190476190476 0.278571428571429
0.0619047619047649],...
  'String','Isentropic Compression',...
  'FitBoxToText','off',...
```

```
  'EdgeColor',[1 1 1]);

figure %isentropic pressure vs isothermal pressure
plot(PR,P2_isent_bar,'r'), hold on
plot(PR,P2_isoth_bar,'b--')
xlim([1.015 13.78])
xlabel 'Pressure Ratio'
ylabel 'p_2 [bars]'
legend('Isentropic','Isothermal','Location','NW')

figure %isentropic compression vs isentropic expansion
plot(PR, work_comp_isentropic,'r'), hold on
plot(PR, work_turb_isentropic,'r--')
xlim([1.015 13.78])
xlabel 'Pressure Ratio', ylabel 'Component Specific Work [kJ/kg]'
annotation('textbox',...
  [0.579571428571428 0.647619047619049 0.313285714285714
0.0642857142857154],...
  'String',{'Isentropic Compression'},...
  'LineStyle','none','FitBoxToText','off');
annotation('textbox',...
  [0.579571428571428 0.219047619047619 0.295428571428572
0.0785714285714291],...
  'String',{'Isentropic Expansion'},...
  'LineStyle','none','FitBoxToText','off');
legend('|_1w_2|','_3w_4','Location','NW')

figure %isentropic vs isothermal processes
plot(PR, work_comp_isentropic,'r'), hold on
plot(PR, work_turb_isentropic,'r--')
plot(PR, work_comp_isothermal,'b-.')

xlim([1.015 13.78])
xlabel 'Pressure Ratio'
ylabel 'Component Specific Work [kJ/kg]'

annotation('textbox',[0.52 0.58 0.32 0.06],'String',...
  {'Isentropic Compression'},...
  'FitBoxToText','off','EdgeColor',[1 1 1]);
annotation('textbox',[0.54 0.24 0.32 0.06],...
  'String',{'Isentropic Expansion'},...
  'LineStyle','none','FitBoxToText','off');
annotation('textbox',[0.46 0.40 0.41 0.057],...
  'String',{'Isothermal Compression/Expansion'},...
  'LineStyle','none','FitBoxToText','off');
annotation('arrow',[0.50 0.50],[0.61 0.51]);
annotation('textbox',[0.43 0.51 0.06 0.05],...
  'String','TES',...
  'LineStyle','none','FitBoxToText','off');
annotation('arrow',[0.45 0.45],[0.31 0.41]);
annotation('textbox',[0.38 0.31 0.06 0.048],...
  'String','TES',...
  'LineStyle','none','FitBoxToText','off');
```

```
legend('|_1w_2|','_3w_4','|_1w_{2t}|=_{2t}w_1',...
  'Location','NW')

figure %Cycle efficiency
plot(PR, CycleEff)
xlim([1 13])
ylim([0 100])
xlabel 'Pressure Ratio', ylabel 'Cycle Efficiency [%]'

%% Calculations for Power Consumption with constant flowrate

% Calculating compressor power consumption to compress tanks to 150
psia
% Mass of air needed at 1034210 Pa (150 psia)
m0 = 1034210*Vtank/(R_air*Tatm);
%Initial volume needed (at Patm and Tatm)
V0 = m0*R_air*Tatm/Patm;
% Seconds of compressor operation to get from initial to final volume
% assuming constant flowrate
sec = floor((V0 - Vtank)/Q);
time_sec = linspace(0,sec,sec);   %Array for time steps of 1 second
time_hour = time_sec/3600;     %Converted to hours for graphing
t_over_tfinal = time_hour/(sec/3600); %Non-dimensionalized
%Establish arrays for pressure and volume values
P_150 = zeros(sec,1); %Array for incremental pressures building up to
       % Psys = 150 psia for isentropic power
P_150_isoth = zeros(sec,1); %Array for incremental pressures building
up to
         % Psys = 150 psia for isothermal power
V_150 = zeros(sec,1); %Array for incremental volumes
%Establish arrays for power and specific power values
Pwr = zeros(sec,1);
specpower = zeros(sec,1);
Pwr_isotherm = zeros(sec,1);
specpower_isotherm = zeros(sec,1);

%Power = P*dV/dt + dP/dt*V
for i = 1:(sec)
  V_150(i) = V0 - Q*i;
  P_150(i) = Patm*((V0/(V0 - Q*i))^n);
  P_150_isoth(i) = Patm*(V0/(V0 - Q*i));
  PxdV_dt = P_150(i)*-1*Q;
  VxdP_dt = (V0-Q*i)*((Patm*Q*V0*n*(V0/(V0-Q*i))^(n-1))/(V0-Q*i)^2);
  mdot = ((P_150(i))^(1/n)*(Patm^((n-1)/n))/(R_air*Tatm))*Q;
  mdot_isotherm = (P_150_isoth(i)/(R_air*Tatm))*Q;
  %Isentropic power calculation
  Pwr(i) = abs((1/(1-n))*(PxdV_dt + VxdP_dt))/1000; %[KW]
  specpower(i) = Pwr(i)/mdot;
  %Isothermal power based on W=P0V0ln(V/V0)
  Pwr_isotherm(i) = abs((Patm*Q*V0)/(V0 - Q*i))/1000;
  specpower_isotherm(i) = Pwr_isotherm(i)/mdot_isotherm;

end
%Convert pressure to bars for graphing
```

```
P_150_bar   = P_150/100000;
P_150_isoth_bar = P_150_isoth/100000;

figure %isentropic vs isothermal power
plot(t_over_tfinal,Pwr,'r'), hold on
plot(t_over_tfinal,Pwr_isotherm,'b--')
xlabel 't/t_f'
ax = gca;
ax.XTick = [0 1];
ylabel 'Compression Power [KW]';
legend('Isentropic Power', 'Isothermal Power', 'Location','NW')

figure %isentropic vs isothermal power
plot(t_over_tfinal,P_150_bar,'r'), hold on
plot(t_over_tfinal,P_150_isoth_bar,'b--')
xlabel 't/t_f'
ax = gca;
ax.XTick = [0 1];
ylabel 'p_2 [bar]';
legend('Isentropic Pressure', 'Isothermal Pressure', 'Location','NW')

figure %isentropic vs isothermal specific power
plot(t_over_tfinal,specpower,'r'), hold on
plot(t_over_tfinal,specpower_isotherm,'b--')
xlabel 't/t_f'
ax = gca;
ax.XTick = [0 1];
ylabel 'Specific Compression Power [KW/kg/s]';
ylim([0 240]);
ax.YTick = [0 80 160 240];
legend('Isentropic Specific Power', 'Isothermal Specific Power',
'Location','NW')

%% Calculations for Power Consumption with capped power supply
% Establishing array of flowrate values. These values will be divided
% by the actual flowrate to obtain a percentage of nominal flowrate
% when compressor power reaches the power supply limit
Qarray_isent = Q*ones(20000000,1);
Qarray_isoth = Q*ones(20000000,1);
%Re-establishing incremental pressure values
P_150_capped = zeros(1400000,1);
P_150_isoth_capped = zeros(1400000,1);

% loop for isentropic capped power
time = 0;    %initialize time
i = 0;     %initialize counter for indexing arrays
while (V0 - Q*i) > Vtank
  i = i + 1;  %increase counter for each loop iteration

  %Isentropic power calculation [KW]
  P_150_capped(i) = Patm*((V0/(V0 - Q*i))^n);
  PxdV_dt = P_150_capped(i)*-1*Q;
  VxdP_dt = (V0-Q*i)*((Patm*Q*V0*n*(V0/(V0-Q*i))^(n-1))/(V0-Q*i)^2);
```

```
  Pwr(i) = abs((1/(1-n))*(PxdV_dt + VxdP_dt))/1000;

  %loop to recalculate power by lowering Q when power is greater than
  %compressor power supply
  while Pwr(i) > pwrmax
   %reducing flowrate
   Q = Q - 0.000000001;
   %calcuate reduced pressure rise
   P_150_capped(i) = Patm*((V0/(V0 - Q*i))^n);
   %calculate power to determine if below max power
   PxdV_dt = P_150_capped(i)*-1*Q;
   VxdP_dt = (V0 - Q*i)*((Patm*Q*V0*n*(V0/(V0 - Q*i))^(n - 1))/(V0 -
Q*i)^2);
   Pwr(i) = abs((1/(1-n))*(PxdV_dt + VxdP_dt))/1000;
  end

  %determine flowrate percentage
  Qarray_isent(i) = (Q/Qarray_isent(i))*100;
  %increase time counter each iteration
  time = time + 1;
end

%convert time to hours array for graphing
time = linspace(0,time,time)/3600;
%non-dimensionalize time with respect to constant flow rate compression
% time
time_over_tfinal = time/(sec/3600);

% loop for isothermal power capped
Q = 0.0028317; %Reset flowrate to nominal value
time1 = 0; %Iniitialize time for isothermal loop
i = 0;  %initialize counter for indexing arrays
while (V0 - Q*i) > Vtank
  i = i + 1;  %increase counter for each loop iteration

  %Isothermal pressure increase
  P_150_isoth_capped(i) = Patm*(V0/(V0 - Q*i));
  %Isothermal power based on W=P0*V0*ln(V/V0)
  Pwr_isotherm(i) = abs((Patm*Q*V0)/(V0 - Q*i))/1000;

  %loop to recalculate power by lowering Q when power is greater than
  %compressor power supply
  while Pwr_isotherm(i) > pwrmax
   %reducing flowrate
   Q = Q - 0.000000001;
   %calcuate reduced pressure rise
   P_150_isoth_capped(i) = Patm*(V0/(V0 - Q*i));
   %calculate power to determine if below max power
   Pwr_isotherm(i) = abs((Patm*Q*V0)/(V0 - Q*i))/1000;
  end
  %determine flowrate percentage
  Qarray_isoth(i) = (Q/Qarray_isoth(i))*100;
  %increase time counter each iteration
  time1 = time1 + 1;
```

```
end

%convert time to hours array for graphing
time1 = linspace(1,time1,time1)/3600;
%non-dimensionalize time with respect to constant flow rate compression
% time
time1_over_tfinal = time1/(sec/3600);
%convert pressure to bars for graphing
P_150_capped = P_150_capped/100000;
P_150_isoth_capped = P_150_isoth_capped/100000;

% Graphing pressure and flow rate under capped power supply conditions
% normalized to constant flow rate compression time

figure %isentropic and isothermal pressure
plot(time_over_tfinal,P_150_capped(1:length(time)),'r-'), hold on
plot(time1_over_tfinal,P_150_isoth_capped(1:length(time1)),'b--')
xlabel 't/t_f' , ylabel 'p_2 [bar]'
legend('Isentropic Pressure','Isothermal Pressure','Location','SE')

figure %isentropic and isothermal flow rates
plot(time_over_tfinal,Qarray_isent(1:length(time)),'r-'), hold on
plot(time1_over_tfinal,Qarray_isoth(1:length(time1)),'b--')
xlabel 't/t_f' , ylabel '% Nominal Flow Rate'
legend('Isentropic Flow Rate','Isothermal Flow Rate')

% Graphing pressure and flow rate under capped power supply conditions
% for estimating time to compress NPS system

figure %isentropic and isothermal pressure
plot(time,P_150_capped(1:length(time)),'r-'), hold on
plot(time1,P_150_isoth_capped(1:length(time1)),'b--')
xlabel 'time [hr]' , ylabel 'p_2 [bar]'
legend('Isentropic Pressure','Isothermal Pressure','Location','SE')

figure %isentropic and isothermal flow rates
plot(time,Qarray_isent(1:length(time)),'r-'), hold on
plot(time1,Qarray_isoth(1:length(time1)),'b--')
ylim([0 100]);
xlabel 'time [hr]' , ylabel '% Nominal Flow Rate'
legend('Isentropic Flow Rate','Isothermal Flow Rate')
```

THIS PAGE INTENTIONALLY LEFT BLANK

LIST OF REFERENCES

[1] Naval Postgraduate School, 2013, "Energy Systems Evaluation Program (ESTEP)," from http://www.nps.edu/Academics/OtherPrograms/Energy/Research/s-t_ESTEP.html

[2] Pollman, A., and Gannon, A., 2015, "Multi-Physics Energy Approach and Demonstration Facility," Power and Energy Conversion, 1(2015), pp. 1–10.

[3] Procon.org, 2013, "Historical Timeline: History of Alternative Energy and Fossil Fuels," from http://alternativeenergy.procon.org/view.timeline.php?timelineID=000015

[4] U.S. Energy Information Administration, 2012, "U.S. Energy Growth Projected to Grow Slowly and Become Less Carbon-Intensive," from http://www.eia.gov/todayinenergy/detail.php?id=4690

[5] Union of Concerned Scientists, 2016, "The Hidden Cost of Fossil Fuels," from http://www.ucsusa.org/clean-energy/coal-and-other-fossil-fuels/hidden-cost-of-fossils#.WCuYV_krLIU

[6] Marris, I., 2015, "Significant Efforts to Reduce Greenhouse Gas Emissions Across UN - New Report," from http://www.unep.org/newscentre/default.aspx?DocumentID=26856&ArticleID=35611

[7] Smick, E., 2006, "U.S. Companies and Greenhouse Gas Regulations," from http://www.cfr.org/united-states/us-companies-greenhouse-gas-regulations/p11462

[8] Office of the Secretary of the Navy, n.d., "Renewable Energy and Sustainability," from http://greenfleet.dodlive.mil/energy/

[9] Deputy Assistant Secretary of the Navy Energy Office, 2012, "Department of the Navy Strategy for Renewable Energy," from http://www.secnav.navy.mil/eie/documents/donstrategyforrenewableenergy.pdf

[10] Commander Navy Region Southwest, 2007, "Regional Energy Management Program," COMNAVREGSWINST 4101.lA, San Diego, CA.

[11] Ash, T., and Erdmann, A., 2013, "Powering the U.S. Military: An Interview with the Pentagon's Sharon Burke," from http://www.mckinsey.com/industries/aerospace-and-defense/our-insights/powering-the-us-military

[12] Kondoh, J., Ishii, I., Yamaguchi, H., 2000, "Electrical Energy Storage Systems for Energy Networks," Energy Conversion and Management, 41(2000), pp. 1863–1874.

[13] Denholm, P., Ela, E., Kirby, B., 2010, "The Role of Energy Storage with Renewable Electricity Generation," Technical Report No. NREL/TP-6A2-47187, National Renewable Energy Laboratory, Golden, CO.

[14] Luo, X., Wang, J., Dooner, M., 2015, "Overview of Current Development in Electrical Energy Storage Technologies and the Application Potential in Power System Operation," Applied Energy, 137(2015), pp. 511–536.

[15] Compressed Air and Gas Institute, 2012, "Working with Compressed Air." from http://www.cagi.org/working-with-compressed-air/applications.aspx

[16] Barnhart, C., and Benson, S., 2013, "On the Importance of Reducing the Energetic and Material Demands of Electrical Energy Storage," Energy and Environmental Science, 6(2013), pp. 1083–1092.

[17] Akhil, A., Huff, G., Currier, A., 2013, "DOE/EPRI 2013 Electricity Storage Handbook in Collaboration with NRECA," Technical Report No. SAND2013-5131, Sandia National Laboratories, Albuquerque, New Mexico and Livermore, California.

[18] energyskeptic, 2016, "Utility Scale Energy Storage Batteries Limited by Materials and Few Locations for Pumped Hydro, Compressed Air," from http://energyskeptic.com/2016/Only-Sodium-Sulfur-Batteries-have-enough-Material-on-Earth-to-Scale-Up/

[19] Grazzini, G., and Milazzo, A., 2008, "Thermodynamic Analysis of CAES/TES Systems for Renewable Energy Plants," Renewable Energy, 33, pp. 1998–2006.

[20] Grazzini, G., and Milazzo, A., 2008, "Exergy Analysis of a CAES with Thermal Energy Storage," Proceedings of the 5th European Thermal Sciences Conference, Eindhoven, The Netherlands, pp. 18–22.

[21] The Arizona Research Institute for Solar Energy, 2010, "Study of Compressed Air Energy Storage with Grid and Photovoltaic Energy Generation," APS Final Draft Report, Compressed Air Energy Storage and Photovoltaics Study, University of Arizona, Tucson, AZ.

[22] Mason, J., Fthenakis, V., Zweibel, K., 2008, "Coupling PV and CAES Power Plants to Transform Intermittent PV Electricity into a Dispatchable Electricity Source," Progress in Photovoltaics: Research and Applications, 16(2008) pp. 649–688.

[23] De Samaniego Steta, F., 2010, "Modeling of an Advanced Adiabatic Compressed Air Energy Storage (AA-CAES) Unit and an Optimal Model-Based Operation Strategy for its Integration into Power Markets." M.S. thesis, Swiss Federal Institute of Technology, Zurich, Switzerland.

[24] Chappell, J., 2011, "A Transient Fluid and Thermodynamic Model of a Compressed Air System," M.S. thesis, Department of Mechanical Engineering, The University of Alabama, Tuscaloosa, AL.

[25] Maxwell, G., and Rivera, P., 2003, "Dynamic Simulation of Compressed Air Systems," ACEEE Summer Study on Energy Efficiency in Industry, pp. 3–146-3-156.

[26] Lawrence Livermore National Laboratory, 2015, "Energy Flow Charts: Charting the Complex Relationships among Energy, Water, and Carbon," from https://flowcharts.llnl.gov

[27] Ter-Gazarian, A., 1994, Energy Storage for Power Systems, Peter Peregrinus Ltd., London, United Kingdom, p. 100, Chap. 7.

[28] Carnegie, R., Gotham, D., Nderitu, D., 2013, "Utility Scale Energy Storage Systems: Benefits, Applications, and Technologies."

[29] EPRI and the U.S. Department of Energy, 2003, "EPRI-DOE Handbook of Energy Storage for Transmission & Distribution Applications," Technical Report No. 1001834, EPRI, Palo Alto, CA and the U.S. Department of Energy, Washington, DC.

[30] Wesoff, E., 2010, "Compressed Air Storage Beats Batteries at Grid Scale," from https://www.greentechmedia.com/Articles/Read/Compressed-Air-Energy-Storage-Beats-Batteries

[31] St. John, J., 2013, "Texas to Host 317 MW of Compressed Air Energy Storage," from https://www.greentechmedia.com/articles/read/texas-calls-for-317mw-of-compressed-air-energy-storage2

[32] Industrialinfo.Com, 2014, "Apex Puts Gas-Fired Bethel Energy Plant in Texas on Hold," http://www.industrialinfo.com/news/abstract.jsp?newsitemID=244860

[33] Yirka, B., 2013, "SustainX Builds 1.5 MW Isotherm Compressed Air Energy Storage System," from http://phys.org/news/2013-09-sustainx-mw-isotherm-compressed-air.html

[34] St. John, J., 2015, "SustainX to Merge with General Compression, Abandon Above-Ground Ambitions," from https://www.greentechmedia.com/articles/read/sustainx-to-merge-with-general-compression-abandon-above-ground-caes-ambiti

[35] LightSail Energy, n.d., “We Store Energy in Compressed Air,” from lightsailenergy.com

[36] St. John, J., 2015, “LightSail’s Secret Plan to Slash the Cost of Compressed Air Energy Storage,” from https://www.greentechmedia.com/articles/read/LightSails-Secret-Plan-to-Slash-the-Costs-of-Compressed-Air-Energy-Storage

[37] Kell, K. M., 2013, “Energy Commission Awards nearly $4 Million for Research Projects,” from http://www.energy.ca.gov/releases/2013_releases/2013 -04-30_4_million_for_research_projects.html

[38] Isentropic, 2015, “Isentropic Ltd Announces Successful Testing of its Layered Thermal Store Prototype,” from http://www.isentropic.co.uk/Publications/News/Successful-Layered-Thermal-Store-Testing

[39] Isentropic, n.d., “Technology,” from http://www.isentropic.co.uk/Technologies

[40] Petrov, M., Arghandeh, R., and Broadwater, R., 2013, “Concept and Application of Distributed Compressed Air Energy Storage Systems Integrated in Utility Networks.” Proc. of the ASME 2013 Power Conference, pp. 1–8.

[41] Kim, Y., Shin, D., and Favrat, D., 2011, “Operating Characteristics of Constant-Pressure Compressed Air Energy Storage (CAES) System Combined with Pumped Hydro Storage Based on Energy and Exergy Analysis,” Energy, 36(2011), pp. 6220–6233.

[42] Kim, Y., Favrat, D., Sin, D., 2010, “Compressed-Air-Storing Electricity Generating System and Electricity Generating Method Using the Same,” U.S. 12/377,866(US7663255 B2).

[43] Sear, J.R., 2005, “Thermal and Compressed-Air Storage (TACAS): The Next Generation of Energy Storage Technology,” Active Power, Austin, TX.

[44] Lemofouet-Gatsi, S., and Rufer, A., 2005, “Hybrid Energy Storage System based on Compressed Air and Super Capacitors with MEPT (Maximum Efficiency Point Tracking),” International Power Electronics Conference, pp. 461–468.

[45] Ibrahima, H., Ilincaa, A., Younèsc, R., 2007, “Study of a Hybrid Wind-Diesel System with Compressed Air Energy Storage,” IEEE Electrical Power Conference, Montreal, Canada.

[46] Langness, C., Kolsky, D., Busch, T., 2013, “Proof-Of-Concept Combined Shrouded Wind Turbine and Compressed Air Energy Storage System,” Proceedings of the ASME 2013 International Mechanical Engineering Congress and Exposition, pp. 1–13.

[47] Paloheimo, H., and Omidiora, M., 2009, "A Feasibility Study on Compressed Air Energy Storage System for Portable Electrical and Electronic Devices," International Conference Clean Electrical Power, pp. 355–362.

[48] Villela, D., Kasinathan, V., De Valle, S., 2010, "Compressed-Air Energy Storage Systems for Stand-Alone Off-Grid Photovoltaic Modules," Photovoltaic Specialists Conference, pp. 962–967.

[49] Kim, Y., 2012, "Novel Concepts of Compressed Air Energy Storage and Thermo-Electric Energy Storage," Ph.D. dissertation, Federal Institute of Technology in Lausanne, Lausanne, France.

[50] Manfrida, G., and Secchi, R., 2014, "Performance Prediction of a Small-Size Adiabatic Compressed Air Energy Storage System," Proceedings of ECOS 2014, pp. 1–15.

[51] Keeney, J., 2013, "Investigation of Compressed Air Energy Storage Efficiency," M.S. thesis, California Polytechnic State University, San Luis Obispo, CA.

[52] Mclaughlin, C., 2016, "Small-Scale Air-Driven Generator," M.S. thesis, Dept. of Mech. Eng., Naval Postgraduate School, Monterey, CA.

[53] Fujiwara, M., Kasuya, K., Matsunaga, T., 1984, "Computer Modeling for Performance Analysis of Rotary Screw Compressor," International Compressor Engineering Conference, pp. 536–543.

[54] Borgnakke, C., and Sonntag, R., 2009, Fundamentals of Thermodynamics, John Wiley & Sons, Inc., Hoboken, NJ, p. 294, Chap. 8.

[55] Home Power, Inc., n.d., "Maximum Power Point Tracking (MPPT)," from http:/www.homepower.com/maximum-power-point-tracking-mppt

[56] Mouser Electronics, n.d., "Maxwell Technologies BMOD0130-P056-B03," from http://www.mouser.com/ProductDetail/Maxwell-Technologies/BMOD0130-P056-B03/?qs=tPRAFY6dJsK7gArBKiC5VA%3d%3d

[57] Powerexinc, n.d., "Compressed Air and Vacuum Pump Technologies," from http://www.powerexinc.com/article/open-oil-less-scroll_176000000000187

[58] Zander, n.d., "Ecodry KA-MT Series – Zander Dryers," from http://www.zandersales.com/ka-mt-dryer.html#simple3

[59] Compressed Air and Gas Institute, n.d., "Types of Compressed Air Dryers Part 2: Refrigerant and Regenerative Desiccant," from http://www.airbestpractices.com/technology/air-treatment/n2/types-compressed-air-dryers-refrigerant-and-regenerative-desiccant

THIS PAGE INTENTIONALLY LEFT BLANK

INITIAL DISTRIBUTION LIST

1. Defense Technical Information Center
   Ft. Belvoir, Virginia

2. Dudley Knox Library
   Naval Postgraduate School
   Monterey, California